Robertson, A.H.F., Emeis, K.-C., Richter, C., and Camerlenghi, A. (Eds.), 1998
Proceedings of the Ocean Drilling Program, Scientific Results, Vol. 160

26. STABLE ISOTOPE AND ALKENONE TEMPERATURE RECORDS OF SAPROPELS FROM SITES 964 AND 967: CONSTRAINING THE PHYSICAL ENVIRONMENT OF SAPROPEL FORMATION IN THE EASTERN MEDITERRANEAN SEA[1]

Kay-Christian Emeis,[2] Hans-Martin Schulz,[2] Ulrich Struck,[2] Tatsuhiko Sakamoto,[3] Heidi Doose,[4] Helmut Erlenkeuser,[5] Michael Howell,[6] Dirk Kroon,[7] and Martine Paterne[8]

ABSTRACT

Sapropels formed in response to changes in the climatic background and in water mass circulation of the Mediterranean Sea. To examine the magnitude of change in surface waters, which are a prominent source of both deep and intermediate waters today, we measured the alkenone unsaturation index of sedimentary lipids (a sea-surface temperature proxy; at Ocean Drilling Program (ODP) Sites 967 and 964, as well as in PALEOFLUX Cores KC01/01B) and the stable oxygen isotope composition of planktonic foraminifers (at Site 967) in closely spaced samples across sapropels. With these data we evaluate the temperature and salinity history of surface waters in Ionian and Levantine Basins of the Eastern Mediterranean at times of sapropel deposition over the last 3 m.y.

Average sea-surface temperatures (SST) are high (23°C) and show little fluctuation in the time interval from 2 to 3 Ma at ODP Site 964 in the Ionian Basin. During this period, we discern no change in the SST going into and out of the sapropel or temperature decreases at the onset of sapropel deposition. Between 0.9 and 1.3 Ma, the average temperatures were between 16°C and 21°C and varied by as much as 6°C within individual sapropel layers. Sapropel SST are markedly higher than those immediately below the organic-rich layers. From 650 ka to the last sapropel (S1) of Holocene age, the average SST across sapropels follow the global climatic background and range from as low as 15°C (during glacial isotope Stage 6) to 21°C (during interglacial isotope Stages 5 and 9), which corresponds to a glacial/interglacial temperature change of 6°C. The ranges of individual SST values are much higher and exceed a 10°C difference between glacial and interglacial samples. Superimposed on the global glacial/interglacial temperature pattern was a warming trend of at least 2°C at the onset of each sapropel event. Temperature gradients between coeval sapropels from the two basins are less than 2°C for the last 400 ka.

Parallel to the warming trends in the sapropels, the $\delta^{18}O$ of planktonic foraminifer calcite decreases by values between 0.7‰ and 3.4‰, of which the temperature change explains only a portion between 0‰ and 1.1‰. The remainder must be caused by salinity and global ice-volume changes of up to 3.4‰ in the surface waters. Published estimates of global ice-volume variations over periods corresponding to individual sapropel intervals account for a maximum of 0.32‰ $\delta^{18}O$ in the change from below to within the sapropels. The corrected isotope data suggest that the surface-water salinity was lower by as much as 7.7 in Sapropel S4 and usually more than 1 for all other sapropels in the late Pleistocene to Holocene. The data validate the hypothesis that the thermohaline circulation was reduced and that the intermediate- and deep-water formation in the Eastern Mediterranean was weakened or impeded.

INTRODUCTION

Rhythmic changes in the physical, chemical, and biological conditions of the Mediterranean Sea are highlighted by sapropel layers in the sediment record. Stratigraphic analyses of land sections and deep-sea cores have established a firm link between sapropel occurrence (and sedimentary cycles without obvious sapropels) and insolation and climatic cycles since the Pliocene and possibly earlier (Lourens et al., 1996; Rossignol-Strick et al., 1982; Cita et al., 1977).

How the climate-sapropel connection works is not yet entirely clear, but most researchers agree that a direct link is most likely established by a change in the physical circulation system in the Mediterranean Sea. Any successful model of sapropel formation must account for the external forcing, for internal dynamics of water-mass circulation, for elevated biological productivity patterns, and for changed properties of water masses in the intermediate- and deep-water layers of the basins (Rohling, 1994; Emeis et al., 1996).

Among the key variables likely responsible for the change in circulation and for sapropel formation is a freshening of surface waters as an expression of changes in the ratio between evaporation (e) and precipitation (p). The value of e/p is presently >1 for the eastern basin (1.6 m of water is annually lost to evaporation in the Levant and precipitation and runoff is only 0.60 m/yr (Béthoux, 1993). The modern circulation pattern is anti-estuarine, and biological productivities in the Eastern Mediterranean are low (Béthoux, 1989). The e/p values may have changed to e/p <1 by increased precipitation, river runoff, or melting of ice during warm and moist climatic conditions, which are associated with many of the sapropels of late Pleistocene and Holocene age (Mommersteeg et al., 1995; Rossignol-Strick, 1993) and with maxima in the insolation. The strongest indication for such a decrease in surface salinity is the pronounced decreases of $\delta^{18}O$ values of planktonic foraminifers found at both the bases of and within sapropels (Vergnaud-Grazzini et al., 1977; Williams and Thunell, 1979). The increased discharge from land—sources under discussion are the Nile, the Black Sea catchment basin, and the northern watershed of the Mediterranean—may have introduced additional nutrients (from river runoff or from reservoirs within the water column) and may have stimulated biological production at the same time when increased stability of the water column prevented or greatly re-

[1]Robertson, A.H.F., Emeis, K.-C., Richter, C., and Camerlenghi, A. (Eds.), 1998. *Proc. ODP, Sci. Results*, 160: College Station, TX (Ocean Drilling Program).

[2]Institut für Ostseeforschung Warnemünde, Seestr. 15, D-18119 Warnemünde, Federal Republic of Germany. kay.emeis@io-warnemuende.de

[3] Graduate School of Science, Hokkaido University, N-10, W-8, Kita-Su, Sapporo, 060, Japan.

[4]GEOMAR Research Center for Marine Geosciences, Wischhofstr. 1-3, D-24148 Kiel, Federal Republic of Germany.

[5]Leibnizlabor für Altersbestimmung und Isotopenforschung, Max-Eydt-str. 11-13, D-24118 Kiel, Federal Republic of Germany.

[6]South Carolina AMP, 300 Main Street, University of South Carolina, Columbia, SC 29208, U.S.A.

[7]Department of Geology and Geophysics, University of Edinburgh, West Mains Road, Edinburgh, United Kingdom.

[8]Centre des Faibles Radioactivités, Gif sur Yvette, France.

duced formation of intermediate- and deep-water masses (Rohling and Gieskes, 1989; Howell and Thunell, 1992). Because oxygen is brought into the intermediate- and deep-water column by newly formed, dense (cold but fresh), deep, and intermediate (warm but salty) waters, oxygen concentrations will be quickly depleted under such conditions. The positive water balance may further have reversed the water flow across the sills and may have created an estuarine circulation system with nutrient build up in the deep and intermediate waters in the eastern basin (Thunell et al., 1984; Sarmiento et al., 1988).

The positive water balance of an estuarine circulation system requires a compensatory flow into the basin, and the inflowing water is from subthermocline levels in the adjacent ocean and is thus cold and nutrient rich. It has been argued that the organic carbon accumulation rates and productivities in sapropels are on the same order of magnitude as those of upwelling areas (Calvert et al., 1992). In extreme cases, such cold and nutrient-rich water may have upwelled in the Eastern Mediterranean Sea and may have led to sapropels by greatly increased productivity levels.

The challenge is to conclusively reconstruct and constrain variability in the physical environment before, during, and after sapropel deposition. In this paper, we present results of investigations on high-resolution samples taken across sapropel intervals in two locations: (1) the Ionian Basin (Site 964 and PALEOFLUX Cores KC01/KC01B) and, (2) the Levantine Basin (Site 967). We measured proxies of sea-surface temperature and salinity in a series of sapropels and in surrounding sediments from the late Pleistocene sequence of S1 to S10 at Site 967 and in a series of Pliocene sapropels recovered at Site 964. The data are applied to test the following hypotheses:

1. Sapropels occur during interglacial and glacial climate phases, and sea-surface temperatures (SST) reflect the insolation as well as the regional ice-cap geography and global climate.

2. Sapropels are always associated with warming phases caused by insolation maxima paced by minima in the precession index. The temperature records of sapropels mirror the insolation.

3. Temperature records in isochronous sapropels from different locations have gradients indicative of upwelling.

4. An initial requirement for sapropel formation is a salinity decrease in the sea surface, and all sapropels are associated with an input of fresh water.

5. The salinity change is of the same magnitude for all sapropels, and all freshwater signals are comparable in their isotopic composition.

Our strategy is to investigate the magnitude of change in SST (and salinity, where data are available) associated with individual sapropels at two locations in the Eastern (Site 967; 34°04.27′N, 32°43.53′E; 2550 m water depth) and in the Central Mediterranean Sea (Site 964; 36°15.63′N, 17°45.01′E; 3660 m water depth). Using these intervals (corresponding to well-constrained time slices), we investigated the relationship between global climate, insolation, and sea-surface conditions at times of sapropel formation over the last 3 m.y. Finally, we use coeval sapropels as end points to see if temperature gradients existed.

METHODS

Samples were obtained from either those taken aboard *JOIDES Resolution* during Leg 160 or in the Bremen Ocean Drilling Program (ODP) Core Repository. On the ship, approximately one-quarter of a core in sapropel intervals and the surrounding sediments was sliced off the working halves, wrapped in plastic, and stored frozen until shipping. In the shore-based laboratory, the quarter cores were cut in 1-cm subsamples and freeze dried. Samples taken in the Core Repository consisted of 1-cm sediment intervals across sapropels and adjoining sediments collected with plastic scoops, which were also freeze dried upon arrival in Warnemünde.

For each sample, we calculated the revised meters composite depth (rmcd) below seafloor based on the tables provided by Sakamoto et al. (Chap. 4, this volume). The rmcd values were then translated into ages based on the rmcd-age relationships given in Howell et al. (Chap. 13, this volume) for Site 964, Kroon et al. (Chap. 14, this volume) for Site 967, and Paterne et al. (unpubl. data) for Cores KC01 and KC01B.

The freeze-dried samples (~2–4 g dry weight) were subsequently split into three subsamples. Two grams were wet sieved to obtain the >125-µm fraction, and the residue was used to pick up to 20 tests (sometimes samples were barren or contained less than 20 tests) of the planktonic foraminifer *Globigerinoides ruber* (white) for isotope analyses. This species is a shallow-dwelling planktonic foraminifer (0–30 m; Hemleben et al., 1989), and the isotope signal of the calcite tests records global ice-volume variations, salinity, and temperature near the sea surface. The isotopic composition of oxygen and carbon in the calcite was analyzed with a Finigan MAT 251 mass spectrometer, and the measurement was calibrated against the Peedee Belemnite (PDB) reference scale through international isotope standards. The isotopic results are expressed in the usual notation $\delta = (R_s/R_{st} - 1) \times 1000$, with R_s and R_{st} denoting the $^{13}C/^{12}C$ or $^{18}O/^{16}O$ ratios in the sample CO_2 and the international standard, respectively. The standard deviation of the isotope analyses is ±0.02‰. At the time of writing, isotope data for sapropel intervals from Site 964 were not yet available.

The second subsample (~1–2 g dry weight) was used to extract lipids and to estimate the alkenone unsaturation index $U^{k'}_{37}$, a SST indicator (Brassell et al., 1986; Emeis et al., 1995). Weighted splits of freeze-dried and homogenized sediments were extracted by ultrasonic agitation with 35-mL CH_2Cl_2 (2 × 10 min). Elemental sulfur was removed by the addition of copper foil during the extraction. After each extraction step, samples were centrifuged, and the solvent was collected by pipette. The two lipid extracts were combined and dried in a rotary evaporator. The extracts were redissolved in CH_2Cl_2 and precleaned over a silica gel column (conditioned with 30-mL CH_2Cl_2) by elution with 14-mL CH_2Cl_2 and dried again in a rotary evaporator. The extracts were redissolved in *n*-hexane and subsequently fractionated using high-pressure liquid chromatography (HPLC). The HPLC column, packed with silica gel, was MERCK, LiChrospher Si 100-5. Four fractions were obtained using 5.5-mL n-hexane, 14-mL *n*-hexane/dichloromethane, 9-mL dichloromethane, and 9-mL acetone as eluents. The ketones (here: alkenones) were isolated in the second fraction. The first fraction contained the aliphatic hydrocarbons, and the third and fourth fractions yielded the more polar compounds.

Gas chromatographic (GC) analyses were carried out on a HR 8000 Fisons gas chromatograph (FID, cold on-column injection) equipped with a 30-m (0.32 mm∅) glass capillary column (DB5HT). Helium was used as a carrier gas (column head pressure 110 kPa). Oven temperature programming conditions were from 35°C to 300°C at 15°C min^{-1} followed by an isothermal period of 15 min at 300°C and from 300°C to 330°C at 15°C min^{-1} followed by an isothermal period of 10 min at 330°C.

Alkenones were identified by comparing retention times with those of synthetic standards. Peak areas were converted to the $U^{k'}_{37}$ index, and SSTs calculated according to a calibration based on culture experiments (Prahl et al., 1988):

$$SST\ (°C) = (C_{37:2} / (C_{37:2} + C_{37:3}) - 0.39) / 0.034.$$

Alkenone concentrations were determined from GC analyses of the ketone fractions based on peak responses relative to 5α-cholestan

as an external standard. Results of triplicate analyses (n = 4) indicate that the standard deviation of temperatures calculated from $U^{k'}_{37}$ is 0.2°C (range 0°C–0.3°C).

The third subsample was used to determine concentrations of organic carbon, total carbon, and total nitrogen. The total carbon and nitrogen contents were determined by combustion at 1200°C under oxygen and detection of CO_2 in an infrared detector using a Metalyt CS 100/1000S and a Heraeus elemental analyzer. Inorganic carbon from carbonates was determined in the same instrument by acidifying subsamples with 17% phosphoric acid under a helium stream and detecting evolving CO_2. Organic carbon was the difference between total and inorganic carbon. Because of limited sample material, we were not able to perform all analyses on all sapropels.

RESULTS

The sapropels investigated are from Site 964 and Cores KC01/01B in the Ionian Sea and Site 967 (Eratosthenes Seamount, Levantine Basin; Fig. 1). The data from Cores KC01/01B (same location as Site 964: 36°15.25′N, 17°44.34′E; 3643 m water depth) have been published elsewhere (Emeis et al., 1996; Doose, unpubl. data). The data on sapropels at Site 967 are presented first, before an attempt is made to reconstruct temperature gradients between the Levantine and Ionian Basins for selected sapropel intervals.

Levantine Sea

According to the stable isotope stratigraphy (Kroon et al., Chap. 14, this volume), the sapropel intervals investigated at Site 967 correspond to the late Pleistocene and Holocene Sapropels S1 through S10, which were deposited since 320 ka. Because the isotope ages assigned to one organic-rich layer between a clear S3 and a clear S5 are too young, S4 may be missing. The environmental record of conditions during deposition of S6 at Site 967 is patchy. First, insufficient tests of *G. ruber* were found to produce a complete isotope record. Secondly, the sapropel was disrupted by several thin mud turbidites. Table 1 gives all analytical results, and Figures 2–10 depict the measured variables ($\delta^{13}C$ and $\delta^{18}O$ of planktonic foraminifer calcite, alkenone SST and alkenone abundance, organic carbon, and nitrogen) vs. age.

The data show that several of the measured variables follow a characteristic pattern in all sapropel intervals at Site 967. The transition from presapropel to sapropel is consistently associated with a significant and rapid decrease in $\delta^{18}O$. The lag between the decrease in the isotopic composition and the beginning of sapropel sedimentation is ~600–1500 yr and is thus within the range observed by Howell and Thunell (1992) for the S1. The range of isotopic values from below to within the sapropel in $\delta^{18}O$ is between –0.67‰ and –3.15‰, and the change to lighter values occurs over less than 1500 yr (Figs. 2–10). Most dramatic is the decrease in Sapropels 2 and 4, with a decrease of $\delta^{18}O$ in excess of –3‰. The sense and magnitude of the temperature change is less consistent between individual sapropels (Figs. 2–10): whereas most sapropels show an increase in the SST values in the lower part and within the sapropels (e.g., S1, S3, S5, S8, S9, and S10) on the order of >2°C, some SST profiles remain at the level that was detected below the sapropel (S2, S7) or even appear to decrease (S4, S6). Values of $\delta^{13}C$ usually vary in concert with $\delta^{18}O$ values (but with reduced amplitudes) and decrease at the beginning of organic-rich sedimentation. Notable exceptions are S2, where $\delta^{13}C$ does not decrease, and S5, where the decrease lowers the $\delta^{13}C$ values by more than 2‰.

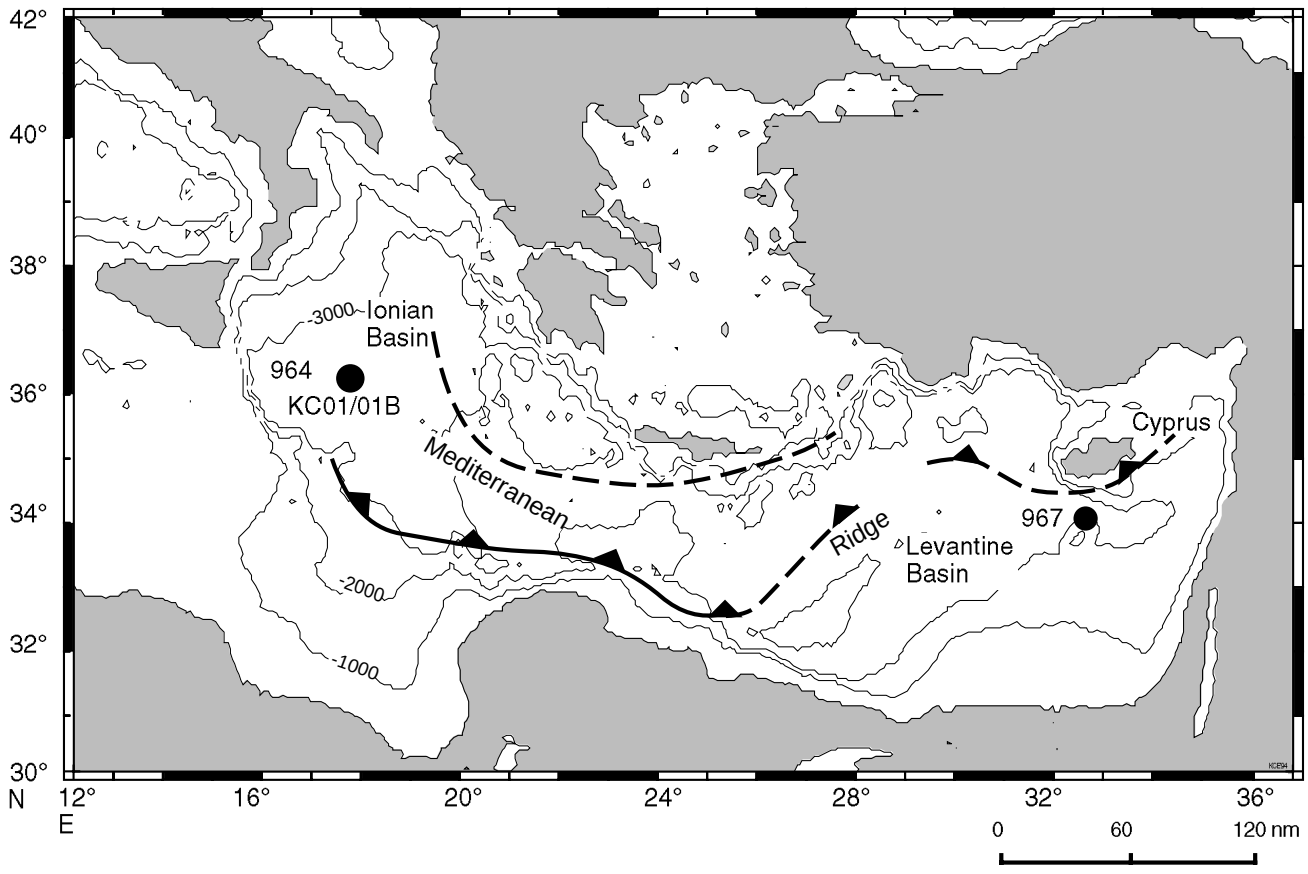

Figure 1. Location map of Sites 967, 964, and Cores KC01/01B in the Eastern Mediterranean Sea.

Table 1. Data for sapropels from Site 967.

Sapropel	Core, section, interval (cm)	Depth (mbsf)	Depth (rmcd)	Age (ka)	$\delta^{13}C$ (‰)	± 1s	$\delta^{18}O$ (‰)	± 1σ	TC (%)	TIC (%)	TN (%)	TOC (%)	$U^{k'}_{37}$	SST (°C)	Σ alkenones (ng/g)
	160-967D-														
S1	1H-1, 100-101	1.00	1.00	7.69	1.10	0.19	–0.30	0.24					0.722	20.1	25
	1H-1, 101-102	1.01	1.01	7.77									0.765	21.4	55
	1H-1, 102-103	1.02	1.02	7.86	1.10	0.02	0.23	0.03					0.699	19.4	29
	1H-1, 103-104	1.03	1.03	7.94	1.13	0.01	0.23	0.02					0.595	16.4	6
	1H-1, 104-105	1.04	1.04	8.03	1.16	0.02	0.22	0.05					0.468	12.6	10
	1H-1, 105-106	1.05	1.05	8.11	1.16	0.02	–0.11	0.04					0.616	17.0	14
	1H-1, 106-107	1.06	1.06	8.20	1.31	0.01	–0.03	0.03					0.556	15.2	7
	1H-1, 107-108	1.07	1.07	8.28	1.53	0.01	–0.11	0.02					0.653	18.1	10
	1H-1, 108-109	1.08	1.08	8.37	1.40	0.01	–0.43	0.02					0.604	16.6	3
	1H-1, 109-110	1.09	1.09	8.45	1.09	0.02	–0.29	0.02					0.573	15.7	9
	1H-1, 110-111	1.10	1.10	8.54	1.40	0.01	–0.55	0.03					0.644	17.8	19
	1H-1, 111-112	1.11	1.11	8.62	1.20	0.02	–0.28	0.02					0.650	18.0	118
	1H-1, 112-113	1.12	1.12	8.71	1.30	0.01	0.06	0.02					0.650	18.0	305
	1H-1, 113-114	1.13	1.13	8.79	1.03	0.01	–0.06	0.03					0.647	17.9	262
	1H-1, 114-115	1.14	1.14	8.87	1.10	0.01	0.05	0.03					0.681	18.9	94
	1H-1, 115-116	1.15	1.15	8.96	0.52	0.02	–0.28	0.02					0.677	18.8	64
	1H-1, 116-117	1.16	1.16	9.04									0.681	18.9	61
	1H-1, 117-118	1.17	1.17	9.13	1.30	0.62	0.92	0.59					0.703	19.5	47
	1H-1, 118-119	1.18	1.18	9.21	0.08	0.01	0.22	0.02					0.657	18.2	426
	1H-1, 119-120	1.19	1.19	9.30	0.84	0.01	–0.27	0.02					0.670	18.6	724
	1H-1, 120-121	1.20	1.20	9.38	0.66	0.02	0.05	0.03					0.670	18.6	412
	1H-1, 121-122	1.21	1.21	9.47	0.60	0.01	–0.10	0.03					0.668	18.5	224
	1H-1, 122-123	1.22	1.22	9.55	0.51	0.02	–0.16	0.02					0.663	18.3	483
	1H-1, 123-124	1.23	1.23	9.64	0.61	0.02	–0.06	0.01					0.664	18.4	506
	1H-1, 124-125	1.24	1.24	9.72	1.08	0.01	–0.38	0.02							
	1H-1, 125-126	1.25	1.25	9.81	0.71	0.02	–0.38	0.03					0.660	18.3	302
	1H-1, 126-127	1.26	1.26	9.89	1.05	0.01	–0.66	0.02							
	1H-1, 127-128	1.27	1.27	9.98	0.49	0.01	–0.05	0.04					0.674	18.7	775
	1H-1, 128-129	1.28	1.28	10.06	0.49	0.02	–0.45	0.02							
	1H-1, 129-130	1.29	1.29	10.15	0.44	0.01	–0.07	0.02					0.657	18.2	553
	1H-1, 130-131	1.30	1.30	10.23	0.45	0.01	–0.25	0.02							
	1H-1, 131-132	1.31	1.31	10.32	0.53	0.01	0.10	0.02					0.599	16.5	16
	1H-1, 132-133	1.32	1.32	10.40	0.61	0.02	0.04	0.03							
	1H-1, 133-134	1.33	1.33	10.49	0.48	0.02	0.39	0.04					0.616	17.0	18
	1H-1, 134-135	1.34	1.34	10.58	0.66	0.01	0.74	0.02							
	1H-1, 135-136	1.35	1.35	10.66	1.02	0.02	1.21	0.04					0.487	13.2	9
S2	1H-3, 120-121	4.20	4.16	58.03	0.77	0.02	1.02	0.03					0.587	16.1	29
	1H-3, 121-122	4.21	4.17	58.22	0.71	0.03	0.58	0.03							
	1H-3, 122-123	4.22	4.18	58.41	0.74	0.04	0.39	0.03					0.643	17.8	26
	1H-3, 123-124	4.23	4.19	58.60	1.28	0.01	0.67	0.03							
	1H-3, 124-125	4.24	4.20	58.79	0.96	0.03	0.78	0.03					0.610	16.8	70
	1H-3, 125-126	4.25	4.21	58.98	0.41	0.55	0.06	0.42							
	1H-3, 126-127	4.26	4.22	59.17	1.07	0.01	0.10	0.02					0.621	17.1	140
	1H-3, 127-128	4.27	4.23	59.36	0.48	0.02	0.08	0.04							
	1H-3, 128-129	4.28	4.24	59.55	0.75	0.01	–0.08	0.02					0.608	16.7	3,387
	1H-3, 129-130	4.29	4.25	59.73	0.95	0.02	–0.25	0.03							
	1H-3, 130-131	4.30	4.26	59.92	0.79	0.02	–0.27	0.03					0.615	17.0	3,718
	1H-3, 131-132	4.31	4.27	60.11	0.72	0.02	–0.47	0.04							
	1H-3, 132-133	4.32	4.28	60.30	0.75	0.03	–0.17	0.06					0.657	18.2	1,114
	1H-3, 133-134	4.33	4.29	60.49	0.68	0.02	–0.14	0.02							
	1H-3, 134-135	4.34	4.30	60.68	0.78	0.02	–0.08	0.02					0.680	18.8	2,188
	1H-3, 135-136	4.35	4.31	60.87	0.33	0.03	–0.11	0.03							
	1H-3, 136-137	4.36	4.32	61.06	0.35	0.03	–0.19	0.04					0.641	17.7	855
	1H-3, 137-138	4.37	4.33	61.25	0.97	0.02	0.31	0.04							
	1H-3, 138-139	4.38	4.34	61.42	0.71	0.03	0.27	0.05					0.664	18.4	69
	1H-3, 139-140	4.39	4.35	61.60	0.83	0.03	–0.04	0.03							
	1H-3, 140-141	4.40	4.36	61.78	0.59	0.01	0.12	0.01					0.579	15.9	8
	1H-3, 141-142	4.41	4.37	61.96	1.38	0.01	2.10	0.02							
	1H-3, 142-143	4.42	4.38	62.14									0.623	17.2	
	1H-3, 143-144	4.43	4.39	62.31	0.73	0.02	0.67	0.08							
	1H-3, 144-145	4.44	4.40	62.49	1.28	0.03	1.89	0.07					0.643	17.8	
	1H-3, 145-146	4.45	4.41	62.67	1.27	0.02	2.86	0.05							
	1H-3, 146-147	4.46	4.42	62.85									0.579	15.9	
	1H-3, 148-149	4.47	4.43	63.03	1.16	0.03	2.96	0.02					0.628	17.3	
	1H-3, 149-150	4.48	4.44	63.20	0.70	0.03	2.60	0.08							
	1H-3, 150-151	4.49	4.45	63.38	1.22	0.02	2.92	0.05					0.644	17.8	
S3	1H-4, 80-81	5.30	5.24	77.46									0.735	20.5	33
	1H-4, 81-82	5.31	5.25	77.64	1.03	0.02	2.01	0.04							
	1H-4, 82-83	5.32	5.26	77.82	1.18	0.01	2.04	0.02					0.744	20.7	20
	1H-4, 83-84	5.33	5.27	78.00	1.11	0.02	0.51	0.02							
	1H-4, 84-85	5.34	5.28	78.17	0.98	0.01	0.37	0.03					0.707	19.6	23
	1H-4, 85-86	5.35	5.29	78.35	0.92	0.02	0.22	0.02							
	1H-4, 86-87	5.36	5.30	78.53	1.01	0.01	0.46	0.03					0.717	20.0	7
	1H-4, 87-88	5.37	5.31	78.71	0.44	0.03	0.45	0.02							
	1H-4, 88-89	5.38	5.32	78.89	0.43	0.02	0.59	0.04					0.691	19.2	13
	1H-4, 89-90	5.39	5.33	79.07	0.37	0.02	0.35	0.04							
	1H-4, 90-91	5.40	5.34	79.25	0.15	0.02	0.87	0.01					0.704	19.6	115
	1H-4, 91-92	5.41	5.35	79.42	1.05	0.01	1.57	0.02							
	1H-4, 92-93	5.42	5.36	79.60	0.76	0.01	1.72	0.03					0.696	19.3	108
	1H-4, 93-94	5.43	5.37	79.78	0.57	0.02	0.59	0.04							
	1H-4, 94-95	5.44	5.38	79.96	0.74	0.02	0.25	0.03					0.709	19.7	588
	1H-4, 95-96	5.45	5.39	80.14	0.83	0.01	0.38	0.03							
	1H-4, 96-97	5.46	5.40	80.32	0.79	0.01	0.31	0.02					0.758	21.1	2,017
	1H-4, 97-98	5.47	5.41	80.49	0.95	0.02	–0.10	0.04							
	1H-4, 98-99	5.48	5.42	80.67	1.05	0.02	0.13	0.03					0.627	17.3	15
	1H-4, 99-100	5.49	5.43	80.85	0.53	0.01	0.70	0.02							
	1H-4, 100-101	5.50	5.44	81.03	0.96	0.01	0.32	0.04					0.645	17.8	6

Table 1 (continued).

Sapropel	Core, section, interval (cm)	Depth (mbsf)	Depth (rmcd)	Age (ka)	$\delta^{13}C$ (‰)	± 1s	$\delta^{18}O$ (‰)	± 1σ	TC (%)	TIC (%)	TN (%)	TOC (%)	$U^{k'}_{37}$	SST (°C)	Σ alkenones (ng/g)
	1H-4, 101-102	5.51	5.45	81.21	0.62	0.03	0.41	0.04							
	1H-4, 102-103	5.52	5.46	81.39	0.86	0.02	0.60	0.04					0.634	17.5	17
	1H-4, 103-104	5.53	5.47	81.57	1.40	0.01	0.61	0.03							
	1H-4, 104-105	5.54	5.48	81.74	1.18	0.02	1.28	0.02					0.600	16.5	9
	1H-4, 105-106	5.55	5.49	81.92	1.01	0.04	1.21	0.04							
	1H-4, 106-107	5.56	5.50	82.10	1.15	0.01	1.28	0.02					0.631	17.4	5
	1H-4, 107-108	5.57	5.51	82.28	1.04	0.02	1.00	0.02							
	1H-4, 108-109	5.58	5.52	82.46	1.16	0.03	0.99	0.02					0.614	16.9	3
	1H-4, 109-110	5.59	5.53	82.64	0.34	0.02	0.51	0.04							
	1H-4, 110-111	5.60	5.54	82.81	0.83	0.03	0.71	0.02					0.721	20.1	30
	1H-4, 111-112	5.61	5.55	82.99	1.24	0.01	0.77	0.03							
	1H-4, 112-113	5.62	5.56	83.17	0.92	0.02	0.82	0.02					0.561	15.3	28
	1H-4, 113-114	5.63	5.57	83.35	1.11	0.02	0.82	0.04							
	1H-4, 114-115	5.64	5.58	83.53	0.99	0.04	0.92	0.05					0.648	17.9	52
	1H-4, 115-116	5.65	5.59	83.70	0.83	0.02	0.31	0.04							
	1H-4, 116-117	5.66	5.60	83.88	0.89	0.02	–0.01	0.04					0.698	19.4	2,394
	1H-4, 117-118	5.67	5.61	84.06	0.23	0.02	–0.36	0.02							
	1H-4, 118-119	5.68	5.62	84.24	0.18	0.03	–0.37	0.03					0.658	18.2	2,266
	1H-4, 119-120	5.69	5.63	84.42	0.62	0.02	–1.19	0.05							
	1H-4, 120-121	5.70	5.64	84.59	0.63	0.02	–1.11	0.03					0.634	17.5	497
	1H-4, 121-122	5.71	5.65	84.77	0.97	0.01	1.22	0.03							
	1H-4, 122-123	5.72	5.66	84.95	1.03	0.02	1.46	0.03					0.718	20.0	76
	1H-4, 123-124	5.73	5.67	85.13	0.74	0.02	1.74	0.01							
	1H-4, 124-125	5.74	5.68	85.30	1.24	0.02	1.75	0.02					0.716	19.9	74
	160-967C-														
S5	1H-5, 68-69	6.68	7.36	117.13	1.26	0.02	1.60	0.03			0.0	0.7	0.760	21.2	466
	1H-5, 69-70	6.69	7.37	117.35	0.45	0.01	–0.11	0.03			0.0	0.6			
	1H-5, 70-71	6.70	7.38	117.58	0.75	0.01	–0.07	0.03			0.0	0.5			
	1H-5, 71-72	6.71	7.39	117.81	0.53	0.02	–0.14	0.03			0.0	0.3	0.733	20.4	47
	1H-5, 72-73	6.72	7.40	118.03	0.68	0.02	–0.23	0.03			0.0	0.8			
	1H-5, 73-74	6.73	7.41	118.26	0.39	0.01	–0.43	0.03			0.0	0.6	0.811	22.7	720
	1H-5, 74-75	6.74	7.42	118.49	–0.16	0.02	–0.03	0.05			0.1	3.2			
	1H-5, 75-76	6.75	7.43	118.71	0.06	0.03	–0.03	0.03			0.1	2.9	0.818	22.9	7,728
	1H-5, 76-77	6.76	7.44	118.94	–0.20	0.03	–0.48	0.04			0.1	3.0			
	1H-5, 77-78	6.77	7.45	119.17	–1.05	0.02	–0.81	0.04			0.0	2.0	0.811	22.7	4,400
	1H-5, 78-79	6.78	7.46	119.39	–1.06	0.01	–1.00	0.03			0.2	3.4			
	1H-5, 79-80	6.79	7.47	119.62	–0.68	0.03	–0.38	0.04			0.1	3.4	0.790	22.1	10,203
	1H-5, 80-81	6.80	7.48	119.85	–0.28	0.02	–0.87	0.04			0.1	3.2			
	1H-5, 81-82	6.81	7.49	120.07	–0.62	0.01	–0.90	0.03			0.1	3.3	0.773	21.6	7,620
	1H-5, 82-83	6.82	7.50	120.30	–0.34	0.02	–0.67	0.04			0.1	3.4			
	1H-5, 83-84	6.83	7.51	120.52	–0.09	0.01	–0.77	0.03			0.1	3.0	0.785	22.0	9,461
	1H-5, 84-85	6.84	7.52	120.75	–0.18	0.03	–0.83	0.04			0.1	2.1			
	1H-5, 85-86	6.85	7.53	120.98	–0.05	0.02	–0.78	0.03			0.1	2.7	0.765	21.4	9,285
	1H-5, 86-87	6.86	7.54	121.20	–0.13	0.02	–0.98	0.06			0.1	2.5			
	1H-5, 87-88	6.87	7.55	121.43	0.04	0.03	–1.07	0.06			0.2	4.3	0.764	21.3	10,056
	1H-5, 88-89	6.88	7.56	121.66	0.11	0.02	–1.23	0.03			0.1	3.2			
	1H-5, 89-90	6.89	7.57	121.88	0.13	0.02	–1.28	0.03			0.1	3.4	0.769	21.5	8,416
	1H-5, 90-91	6.90	7.58	122.11	0.10	0.02	–1.53	0.03			0.1	3.0			
	1H-5, 91-92	6.91	7.59	122.34	0.20	0.02	–1.22	0.02			0.1	3.2	0.771	21.5	7,481
	1H-5, 92-93	6.92	7.60	122.56	–0.11	0.02	–1.01	0.03			0.2	4.2			
	1H-5, 93-94	6.93	7.61	122.79	0.44	0.02	–1.80	0.03			0.2	4.3	0.772	21.6	13,842
	1H-5, 94-95	6.94	7.62	123.02	0.16	0.03	–1.42	0.04			0.1	2.5			
	1H-5, 95-96	6.95	7.63	123.24	0.04	0.02	–1.84	0.03			0.2	4.5	0.728	20.3	11,008
	1H-5, 96-97	6.96	7.64	123.47	0.23	0.02	–1.66	0.02			0.2	3.8			
	1H-5, 97-98	6.97	7.65	123.69	0.56	0.01	–1.91	0.02			0.1	2.9	0.720	20.0	8,495
	1H-5, 98-99	6.98	7.66	123.96	0.89	0.02	–1.29	0.02			0.1	3.1			
	1H-5, 99-100	6.99	7.67	124.22	0.49	0.01	–1.60	0.03			0.2	2.8	0.687	19.1	3,567
	1H-5, 100-101	7.00	7.68	124.49	0.53	0.01	–1.65	0.02			0.1	2.1			
	1H-5, 101-102	7.01	7.69	124.76	0.67	0.02	–1.54	0.03			0.1	2.0	0.684	19.0	2,012
	1H-5, 102-103	7.02	7.70	125.02	0.23	0.02	–1.28	0.02			0.1	1.7			
	1H-5, 103-104	7.03	7.71	125.29	0.68	0.01	–1.08	0.02			0.1	1.0	0.644	17.8	216
	1H-5, 104-105	7.04	7.72	125.55	0.23	0.03	–1.45	0.04			0.0	0.6			
	1H-5, 105-106	7.05	7.73	125.82	0.21	0.02	–1.18	0.02			0.1	1.1	0.588	16.1	27
	1H-5, 106-107	7.06	7.74	126.08	0.55	0.02	–0.11	0.03			0.0	0.6			
	1H-5, 107-108	7.07	7.75	126.35	1.30	0.01	–0.10	0.04			0.0	0.4	0.645	17.8	46
	1H-5, 108-109	7.08	7.76	126.62	1.48	0.02	–0.04	0.01			0.0	0.3			
	1H-5, 109-110	7.10	7.77	126.88	1.21	0.03	–0.12	0.03			0.0	0.3	0.670	18.6	51
S6	2H-1, 130-131	8.00	9.30	164.87	0.93	0.04	1.22	0.02					0.575	15.8	37
	2H-1, 131-132	8.01	9.31	165.14	0.89	0.01	1.28	0.05							
	2H-1, 132-133	8.02	9.32	165.42	0.64	0.03	1.09	0.04					0.644	17.8	4
	2H-1, 133-134	8.03	9.33	165.69	0.76	0.02	1.06	0.02							
	2H-1, 134-135	8.04	9.34	165.96	0.54	0.03	0.43	0.05					0.673	18.6	52
	2H-1, 135-136	8.05	9.35	166.24	0.74	0.02	0.96	0.02							
	2H-1, 136-137	8.06	9.36	166.51	1.01	0.02	0.44	0.03					0.601	16.5	49
	2H-1, 137-138	8.07	9.37	166.78	1.05	0.01	1.23	0.03							
	2H-1, 138-139	8.08	9.39	167.06	0.73	0.02	1.01	0.03					0.584	16.0	38
	2H-1, 139-140	8.09	9.40	167.33	0.53	0.02	1.61	0.02							
	2H-1, 140-141	8.10	9.41	167.60	0.51	0.03	1.66	0.05					0.585	16.1	6,166
	2H-1, 141-142	8.11	9.42	167.84	0.97	0.03	0.73	0.05							
	2H-1, 142-143	8.12	9.43	168.09									0.594	16.3	6,741
	2H-1, 143-144	8.13	9.44	168.33											
	2H-1, 144-145	8.14	9.45	168.57									0.601	16.5	14,068
	2H-1, 145-146	8.15	9.46	168.81											
	2H-1, 146-147	8.16	9.47	169.05									0.550	15.0	6,946
	2H-1, 148-149	8.18	9.49	169.54									0.533	14.5	1,434
	2H-2, 1-2	8.21	9.51	170.27									0.513	13.9	9,862
	2H-2, 3-4	8.23	9.53	170.76									0.521	14.2	14,898
	2H-2, 5-6	8.25	9.55	171.25									0.481	13.0	7,073
	2H-2, 7-8	8.27	9.57	171.74									0.498	13.5	7,359
	2H-2, 9-10	8.29	9.59	172.23									0.531	14.5	12,866

Table 1 (continued).

Sapropel	Core, section, interval (cm)	Depth (mbsf)	Depth (rmcd)	Age (ka)	$\delta^{13}C$ (‰)	± 1s	$\delta^{18}O$ (‰)	± 1σ	TC (%)	TIC (%)	TN (%)	TOC (%)	$U_{37}^{k'}$	SST (°C)	Σ alkenones (ng/g)
	2H-2, 11-12	8.31	9.61	172.72									0.501	13.6	13,364
	2H-2, 13-14	8.33	9.63	173.21									0.575	15.8	8,932
	2H-2, 15-16	8.35	9.65	173.70									0.490	13.3	12,400
	2H-2, 17-18	8.37	9.67	174.19									0.474	12.8	11,870
	2H-2, 19-20	8.39	9.69	174.68									0.458	12.3	1,640
	2H-2, 21-22	8.41	9.71	175.17									0.490	13.3	20,183
	2H-2, 23-24	8.43	9.73	175.66					7.2	4.3	0.2	2.9	0.551	15.1	11,391
	2H-2, 24-25	8.44	9.74	175.90					8.2	4.0	0.3	4.2			
	2H-2, 25-26	8.45	9.75	176.14					2.6	1.2	0.1	1.5	0.532	14.5	3,123
	2H-2, 26-27	8.46	9.76	176.39					2.3	0.7	0.1	1.6			
	2H-2, 27-28	8.47	9.77	176.64					1.4	0.6	0.1	0.8	0.614	16.9	209
	2H-2, 29-30	8.49	9.79	177.12					7.4	2.7	0.2	4.7	0.511	13.9	8,634
	2H-2, 31-32	8.51	9.81	177.61					1.7	0.8	0.1	0.9	0.582	16.0	954
	2H-2, 33-34	8.53	9.83	178.10					1.7	0.8	0.1	0.9	0.629	17.4	567
	2H-2, 35-36	8.55	9.85	178.59					7.8	5.2	0.2	2.5	0.550	15.0	11,164
	2H-2, 37-38	8.57	9.86	179.07					5.9	4.2	0.1	1.7	0.629	17.4	2,176
	2H-2, 39-40	8.59	9.88	179.56					3.9	3.2	0.1	0.7	0.632	17.5	207
	2H-2, 41-42	8.61	9.90	180.07					4.0	2.9	0.1	1.1	0.576	15.8	968
S7	2H-2, 130-131	9.50	10.69	199.83	1.17	0.01	1.21	0.03	4.2	3.4	0.1	0.8	0.587	16.1	243
	2H-2, 131-132	9.51	10.70	200.16	0.56	0.01	1.50	0.02							
	2H-2, 132-133	9.52	10.71	200.50	1.10	0.02	0.94	0.03	5.0	3.9	0.1	1.1	0.668	18.5	931
	2H-2, 133-134	9.53	10.72	200.83	0.73	0.03	1.47	0.04							
	2H-2, 134-135	9.54	10.73	201.17	0.51	0.02	0.90	0.04	7.9	3.7	0.2	4.2	0.686	19.0	6,582
	2H-2, 135-136	9.55	10.74	201.50	0.60	0.02	0.75	0.03							
	2H-2, 136-137	9.56	10.75	201.84	0.37	0.01	1.29	0.02	9.0	3.6	0.3	5.4	0.691	19.2	16,545
	2H-2, 137-138	9.57	10.76	202.17	0.01	0.01	0.87	0.02							
	2H-2, 138-139	9.58	10.77	202.51	0.40	0.02	–0.43	0.05	9.0	4.1	0.3	4.9	0.707	19.6	12,739
	2H-2, 139-140	9.59	10.78	202.86	0.36	0.02	0.27	0.01							
	2H-2, 140-141	9.60	10.79	203.21	0.38	0.02	0.22	0.02	9.9	3.8	0.4	6.1	0.703	19.5	16,726
	2H-2, 141-142	9.61	10.81	203.73											
	2H-2, 142-143	9.62	10.82	204.25	–0.39	0.05	–0.06	0.06					0.688	19.1	21,872
	2H-2, 143-144	9.63	10.83	204.59	0.30	0.02	–0.15	0.02	10.7	3.6	0.4	7.1			
	2H-2, 144-145	9.64	10.84	204.92	0.26	0.03	–1.94	0.05	10.7	3.6	0.4	7.1	0.695	19.3	18,298
	2H-2, 145-146	9.65	10.85	205.27	0.46	0.02	–0.95	0.04							
	2H-2, 146-147	9.66	10.86	205.62	0.50	0.02	–0.94	0.02	9.3	3.8	0.4	5.6	0.694	19.3	9,746
	2H-2, 147-148	9.67	10.87	205.98	0.66	0.02	–1.74	0.03							
	2H-2, 148-149	9.68	10.88	206.33	0.77	0.02	–1.37	0.04	6.6	3.4	0.2	3.2	0.724	20.1	7,981
	2H-2, 149-150	9.69	10.89	206.53	0.69	0.01	–1.22	0.02							
	2H-3, 0-1	9.70	10.90	206.73	0.67	0.04	–0.54	0.05	6.1	3.3	0.2	2.8	0.754	21.0	5,300
	2H-3, 1-2	9.71	10.91	207.07	0.55	0.02	–0.41	0.04	5.4	3.1	0.2	2.4	0.751	20.9	4,151
	2H-3, 2-3	9.72	10.92	207.40	0.39	0.01	0.30	0.03	2.8	1.6	0.1	1.2	0.726	20.2	1,064
	2H-3, 3-4	9.73	10.93	207.74	0.53	0.01	0.49	0.02	2.0	1.1	0.1	0.9	0.702	19.5	414
S7	2H-3, 23-25	9.93	11.13	216.80	0.72	0.02	0.48	0.03							
	2H-3, 25-27	9.95	11.15	217.79	0.90	0.02	0.14	0.05							
	2H-3, 27-28	9.97	11.17	218.74	1.09	0.01	1.32	0.02							
	2H-3, 29-30	9.99	11.19	219.73	1.40	0.02	1.28	0.05							
S8	2H-3, 60-61	10.30	11.50	234.38	1.09	0.01	–0.23	0.02					0.704	19.6	80
	2H-3, 61-62	10.31	11.51	234.66	0.85	0.03	–0.23	0.03							
	2H-3, 62-63	10.32	11.52	234.99	1.34	0.01	0.11	0.03					0.744	20.7	37
	2H-3, 63-64	10.33	11.52	235.28	0.90	0.01	–0.24	0.04							
	2H-3, 64-65	10.34	11.53	235.61	0.89	0.01	–0.22	0.02					0.759	21.2	68
	2H-3, 65-66	10.35	11.53	235.90	0.96	0.02	–0.74	0.01							
	2H-3, 66-67	10.36	11.54	236.23	0.95	0.01	–0.64	0.03					0.755	21.1	778
	2H-3, 67-68	10.37	11.55	236.51	0.89	0.01	–0.78	0.02							
	2H-3, 68-69	10.38	11.55	236.85	0.94	0.01	–0.53	0.02							
	2H-3, 69-70	10.39	11.56	237.18	1.16	0.01	–0.91	0.03							
	2H-3, 70-71	10.40	11.57	237.46	1.04	0.01	–0.84	0.02					0.691	19.2	291
	2H-3, 71-72	10.41	11.57	237.80	1.06	0.02	–1.10	0.03							
	2H-3, 72-73	10.42	11.58	238.01	0.89	0.01	–0.61	0.03					0.650	18.0	139
	2H-3, 73-74	10.43	11.59	238.19	0.49	0.02	–1.05	0.02							
	2H-3, 74-75	10.44	11.59	238.34	1.17	0.01	–0.87	0.03					0.602	16.6	556
	2H-3, 75-76	10.45	11.60	238.52	1.01	0.02	–1.11	0.03							
	2H-3, 76-77	10.46	11.61	238.67	0.97	0.02	–1.00	0.03					0.610	16.8	1,280
	2H-3, 77-78	10.47	11.61	238.85	0.90	0.02	–1.17	0.03							
	2H-3, 78-79	10.48	11.62	239.00	0.96	0.02	–0.52	0.03					0.614	16.9	3,274
	2H-3, 79-80	10.49	11.63	239.18	0.80	0.01	–1.25	0.02							
	2H-3, 80-81	10.50	11.63	239.36	0.36	0.01	–0.79	0.03					0.604	16.6	5,115
	2H-3, 81-82	10.51	11.64	239.51									0.607	16.7	5,339
	2H-3, 83-84	10.53	11.65	239.84									0.628	17.3	3,375
	2H-3, 85-86	10.55	11.67	240.17									0.643	17.8	13,031
	2H-3, 87-88	10.57	11.68	240.50									0.633	17.5	4,987
	2H-3, 88-89	10.58	11.69	240.68											
	2H-3, 89-90	10.59	11.69	240.83									0.609	16.8	9,746
	2H-3, 90-91	10.60	11.70	241.01											
	2H-3, 91-92	10.61	11.71	241.19									0.638	17.6	1,303
	2H-3, 92-93	10.62	11.71	241.34											
	2H-3, 93-94	10.63	11.72	241.52									0.547	14.9	618
	2H-3, 94-95	10.64	11.72	241.67											
	2H-3, 95-96	10.65	11.73	241.85									0.554	15.1	1,555
	2H-3, 96-97	10.66	11.74	242.00											
	2H-3, 97-98	10.67	11.74	242.18									0.528	14.4	6,155
	2H-3, 98-99	10.68	11.75	242.33											
	2H-3, 99-100	10.69	11.76	242.51									0.513	13.9	5,431
	2H-3, 100-101	10.70	11.76	242.66											
	2H-3, 101-102	10.71	11.77	242.84									0.528	14.4	5,900
	2H-3, 102-103	10.72	11.78	243.02	0.85	0.02	–1.16	0.05							
	2H-3, 103-104	10.73	11.78	243.17	1.03	0.03	–1.04	0.03					0.479	12.9	368
	160-968D- 2H-3, 104-105	10.74	11.79	243.43	1.13	0.02	–0.35	0.02							

Table 1 (continued).

Sapropel	Core, section, interval (cm)	Depth (mbsf)	Depth (rmcd)	Age (ka)	$\delta^{13}C$ (‰)	± 1s	$\delta^{18}O$ (‰)	± 1σ	TC (%)	TIC (%)	TN (%)	TOC (%)	$U^{k'}_{37}$	SST (°C)	Σ alkenones (ng/g)
	160-969D-														
	2H-3, 105-106	10.75	11.80	243.50	0.74	0.02	–0.72	0.03					0.525	14.3	173
	160-970D-														
	2H-3, 106-107	10.76	11.80	243.67											
	160-971D-														
	2H-3, 107-108	10.77	11.81	243.83									0.641	17.7	147
	160-972D-														
	2H-3, 108-109	10.78	11.82	244.00	0.71	0.01	–0.47	0.02							
	160-967D-														
	2H-3, 109-110	10.79	11.82	244.16	0.66	0.02	–0.21	0.03					0.613	16.9	55
S9	2H-3, 140-141	11.10	12.09	250.17	0.84	0.03	–0.71	0.03					0.665	18.4	15
	2H-3, 141-142	11.11	12.10	250.40	0.74	0.02	–0.64	0.03					0.662	18.3	8
	2H-3, 142-143	11.12	12.11	250.61	0.69	0.01	–0.56	0.03					0.730	20.3	13
	2H-3, 143-144	11.13	12.13	250.85	0.87	0.01	–1.09	0.02					0.730	20.3	16
	2H-3, 144-145	11.14	12.14	251.06	0.92	0.02	–0.75	0.03					0.768	21.4	16
	2H-3, 145-146	11.15	12.15	251.30	0.89	0.01	–0.68	0.04					0.760	21.2	24
	2H-3, 146-147	11.16	12.16	251.51	0.91	0.01	–0.83	0.03					0.768	21.4	46
	2H-3, 147-148	11.17	12.17	251.72	0.43	0.02	–0.90	0.02					0.761	21.2	594
	2H-3, 148-149	11.18	12.18	251.95	0.53	0.01	–0.95	0.03					0.739	20.6	3,311
	2H-3, 149-150	11.19	12.19	252.17	0.58	0.01	–0.78	0.03					0.761	21.2	2,889
	2H-4, 0-1	11.20	12.20	252.40	0.36	0.01	–0.74	0.02					0.755	21.1	2,007
	2H-4, 1-2	11.21	12.21	252.62	0.50	0.01	–0.69	0.02					0.732	20.4	2,224
	2H-4, 2-3	11.22	12.22	252.85	0.83	0.02	–1.02	0.03					0.736	20.5	865
	2H-4, 3-4	11.23	12.23	253.07	0.94	0.01	–1.02	0.03					0.734	20.4	170
	2H-4, 4-5	11.24	12.24	253.30	0.80	0.02	–0.29	0.05					0.749	20.9	58
	2H-4, 5-6	11.25	12.25	253.54	1.46	0.01	0.21	0.02					0.689	19.1	66
	2H-4, 6-7	11.26	12.26	253.75	1.65	0.01	–0.04	0.03					0.644	17.8	73
	2H-4, 7-8	11.27	12.27	253.99	1.46	0.01	0.22	0.02					0.687	19.0	91
	2H-4, 8-9	11.28	12.28	254.23	1.52	0.02	0.27	0.02							
	2H-4, 9-10	11.29	12.29	254.44	0.87	0.03	0.52	0.03					0.611	16.8	46
S10	2H-5, 125-126	13.95	14.96	320.60	0.70	0.01	–0.05	0.01					0.701	19.5	12
	2H-5, 126-127	13.96	14.97	320.84	0.46	0.01	–0.78	0.02					0.729	20.3	8
	2H-5, 127-128	13.97	14.98	321.10	0.33	0.02	–0.64	0.05							
	2H-5, 128-129	13.98	14.99	321.34	0.35	0.02	–0.66	0.04					0.826	23.1	16
	2H-5, 129-130	13.99	15.00	321.60	0.63	0.01	–0.90	0.02							
	2H-5, 130-131	14.00	15.01	321.84											
	2H-5, 131-132	14.01	15.02	322.10	0.63	0.01	–0.89	0.02					0.807	22.6	87
	2H-5, 132-133	14.02	15.03	322.34	0.43	0.01	–1.05	0.03					0.784	21.9	543
	2H-5, 133-134	14.03	15.04	322.60	0.48	0.02	–1.21	0.03					0.779	21.8	3,113
	2H-5, 134-135	14.04	15.05	322.84	0.48	0.01	–1.13	0.02					0.774	21.6	1,236
	2H-5, 135-136	14.05	15.06	323.10	0.55	0.02	–1.19	0.01					0.777	21.7	1,364
	2H-5, 136-137	14.06	15.06	323.34	0.78	0.01	–1.19	0.02					0.776	21.7	1,004
	2H-5, 137-138	14.07	15.07	323.60	0.40	0.01	–1.09	0.02					0.780	21.8	1,605
	2H-5, 138-139	14.08	15.08	323.84	0.60	0.02	–1.32	0.03					0.757	21.1	1,718
	2H-5, 139-140	14.09	15.09	324.10	0.73	0.02	–1.18	0.03					0.769	21.5	1,426
	2H-5, 140-141	14.10	15.10	324.34	0.65	0.01	–1.25	0.03					0.742	20.7	369
	2H-5, 141-142	14.11	15.11	324.58	0.88	0.01	–0.97	0.04					0.759	21.2	236
	2H-5, 142-143	14.12	15.12	324.81	0.81	0.03	–0.75	0.04					0.775	21.7	113
	2H-5, 143-144	14.13	15.13	325.05	0.77	0.01	–0.54	0.02					0.691	19.2	82
	2H-5, 144-145	14.14	15.14	325.32	0.39	0.02	–0.37	0.03					0.673	18.6	85

Notes: Ages are interpolated from revised meters composite depth (rmcd; Sakamoto et al., Chap. 4, this volume) and the isotope age model of Kroon et al. (Chap. 14, this volume). The columns $\delta^{13}C$ and $\delta^{18}O$ contain the isotopic composition of *Globigerinoides ruber* calcite. TC = total carbon concentrations, TIC = total inorganic carbon concentrations, TN = total nitrogen concentrations, TOC = total organic carbon concentrations. Σ alkenones = the concentration of total extractable alkenones in the sample.

Ionian Basins

One of the Ionian Basin SST records is from Core KC01/01B, which dates back 1.1 m.y. and includes 15 sapropel layers (Castradori, 1993; Sanvoisin et al., 1993). For this core, a high-resolution isotope stratigraphy has been established (Paterne, unpubl. data), and we have measured the alkenone unsaturation indexes within the sapropel layers. The location of the core is the same as for ODP Site 964 (see Fig. 1). In addition, we have determined the alkenone unsaturation index for a total of 17 sapropel intervals at Site 964. For this site, Howell et al. (Chap. 13, this volume) produced an isotope stratigraphy. Table 2 lists the data for sapropels from Site 964.

Figures 11A–11G depict the SST curves for those sapropels measured at Sites 967 and 964. At this preliminary stage of the stratigraphic analyses, differences and uncertainties in the age models used here result in lags or leads of individual sapropel events at one site when compared to other sites. Detailed analyses will prove if they are indeed isochronous, but for the time being we assume that their bases are isochronous, and we adjusted their bases to coincide with the ages derived at Site 967 (which agree well with the ages in Lourens et al., 1996) to more easily compare the temperature variations.

In Ionian Basin Core KC01, S1 (Fig. 11A) lacks a clear warming trend at the base of the sapropel interval. The average temperature within the sapropel is very uniform at 17.1°C ± 1.1°C and is up to 2°C colder than at Site 967 at the center of the sapropel. Temperatures were very uniform during deposition of S4 in the Ionian Sea (Fig. 11B), and the data indicate no gradient between the Ionian and Levantine sites at that time. In contrast, S5 shows inverse temperature trends from a clear increase at Site 967 to a decreasing trend from 22°C to 17°C in the Ionian Basin core (Fig. 11C). The average temperature of S5 is 20.1°C in the Central Mediterranean, with a standard deviation of 2.0°C. In both locations, the total temperature range is in excess of 6°C.

In both locations, S6 is cold with minima below 12°C; the average SST in the Ionian Basin during S6 deposition was 14°C ± 1.5°C (Fig. 11D). In the upper portion of the sapropel, the SST estimates at Site 967 are significantly higher (by ~2°C) than in Core KC01. In contrast, S7 was warm at both locations and averaged 20.7°C ± 2.2°C in the Ionian Basin; the temperature difference was insignificant between the eastern and western location during its deposition (Fig. 11E).

As a test, if the sapropel records in both cores of the Ionian Basin site are comparable, we selected one of the young sapropels that had previously been investigated in both Core KC01B and Hole 964E (160-964E-2H-1, 133 cm) for high-resolution analyses. From the core stratigraphy of Core KC01B, the sapropel is S8. Figure 11F plots

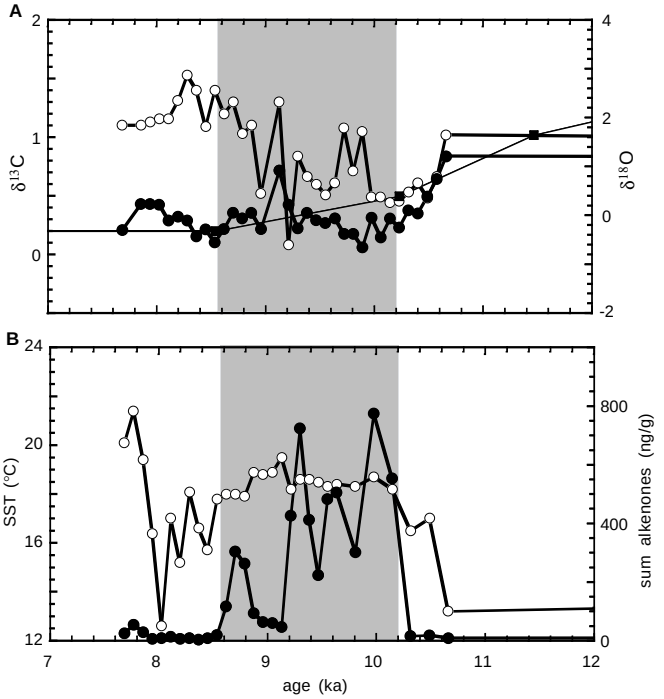

Figure 2. Plot of data for interval 160-967D-1H-1, 100–136 cm. The depth interval of S1 is shaded. **A.** Isotope ratios $\delta^{13}C$ (open circles) and $\delta^{18}O$ (solid circles) of calcite from tests of the planktonic foraminifer *Globigerinoides ruber* (White). Solid squares are data points of the isotope curve presented in Kroon et al. (Chap. 14, this volume) for the location. **B.** Sea-surface temperature (SST) estimates from U^{k}_{37} values (open circles) and concentration of alkenones (ng/g sediment; solid circles). The alkenone concentrations indicate the extent of the organic-rich sapropel layer.

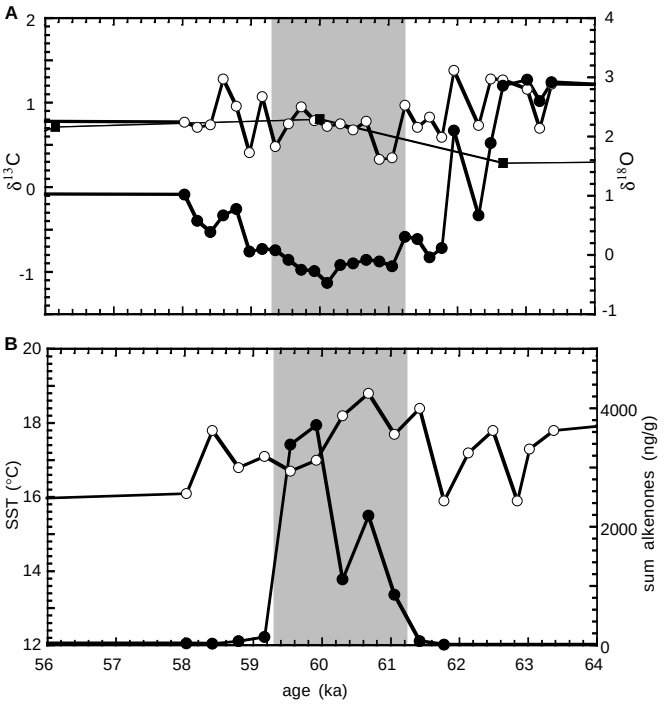

Figure 3. Plot of data for interval 160-967D-1H-3, 120–151 cm. The depth interval of S2 is shaded. Variables plotted as in Figure 2.

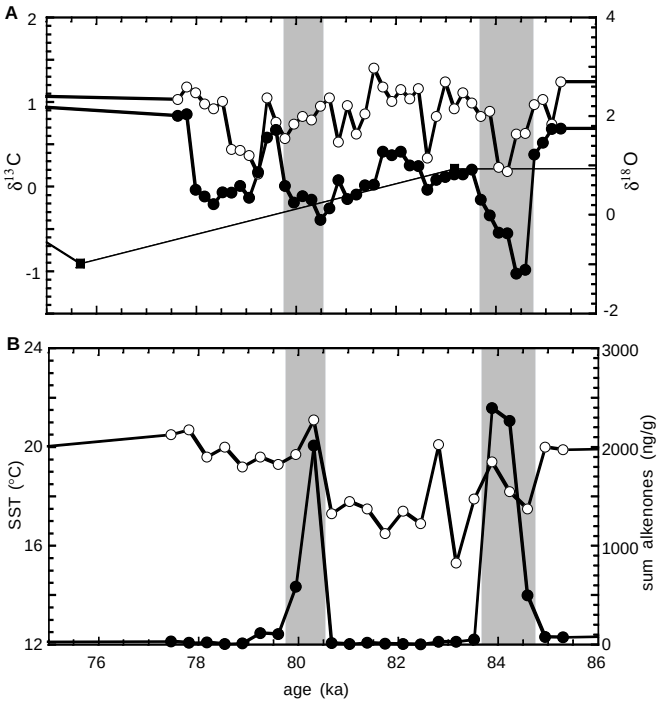

Figure 4. Plot of data for interval 160-967D-1H-4, 80–125 cm. The depth interval of S3, and possibly S4, is shaded. Variables plotted as in Figure 2.

the SST measurements at the three locations, Site 967, Core KC01B, and Site 964, on a common age scale that was adjusted so that the base of S8 begins at 243 ka. Over the sapropel interval, the SST at the three locations shows very similar trends and amplitudes in absolute SST: they increase steadily by 7°C from 11°C to 18°C at Site 964 and Core KC01B and from 13°C to 21°C at Site 967 in the Levantine Basin. The results show very similar SST curves of warming at the base of the sapropel layer, little temperature difference in the first half of the sapropel when temperatures were below 16°C, and a progressive divergence to warmer temperatures in the Levantine Basin (>20°C) as compared to the Ionian Basin (18°C) in the upper part of the sapropel. Even internal features, such as a plateau in SST in the middle of the sapropel, are present in all three intervals. The two high-resolution SST time series of Sapropel S8 yield near-identical results for two cores at one location (the Ionian Basin) and surprisingly similar trends in the eastern and central basins of the Mediterranean Sea.

The last of the sapropels analyzed in Core KC01B is S9 (Fig. 11G), and the data suggest that the temperature conditions at the sea surface were very similar in the Ionian and Levantine Basins with SST in the sapropel interval at 18°C–22°C.

The older sapropel intervals analyzed from Site 964 (older than S10) do not yet have measured counterparts in the Levantine Basin site. In the sapropels that date from 490 to 2310 ka, according to the stratigraphies of Howell et al. (Chap. 13, this volume) and Di Stefano (Chap. 8, this volume), the pattern of rising temperatures coinciding with the onset of sapropel deposition is repeated (Figs. 12–22). The base level of SST varies between 12°C and 20°C, and the range of temperature increase is between 4°C and 8°C; both features have also been seen in the sapropels from the late Quaternary group. Only the three oldest sapropels investigated at Site 964 (>2.6 Ma) differ in their relationship between SST and onset of sapropel formation. In all three cases (Figs. 23, 24, and 25) investigated so far, the SST remain high, and either unchanged at around 22°C, or show an uncharacteristic decrease in the thin sapropel intervals. The temperature range is also reduced in these old sapropels: SST estimates vary between

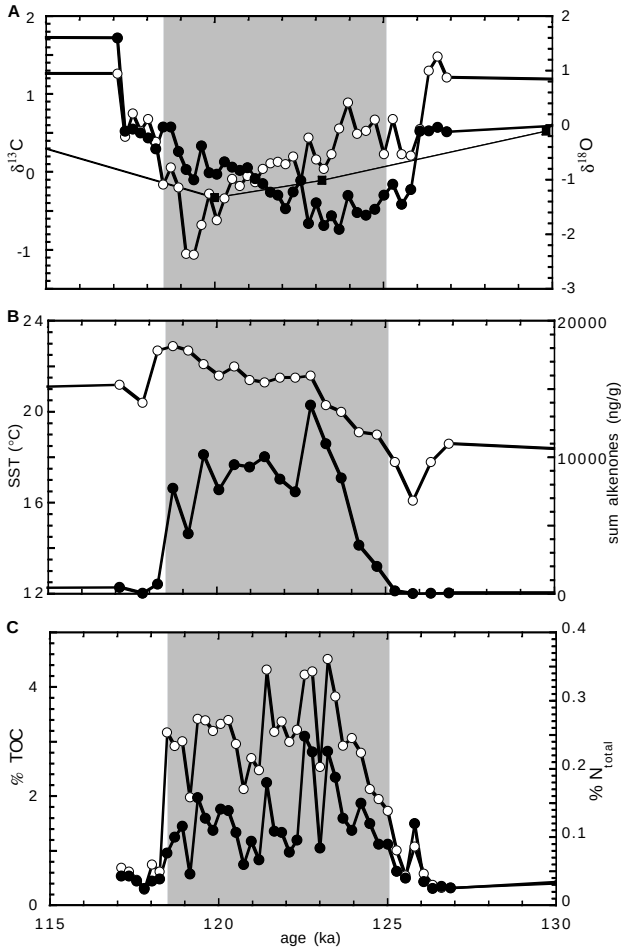

Figure 5. Plot of data for interval 160-967C-1H-5, 68–110 cm. **A–B.** The depth interval of S5 is shaded. Variables plotted as in Figure 2. **C.** Organic carbon concentrations (open circles) and total nitrogen concentrations (solid circles).

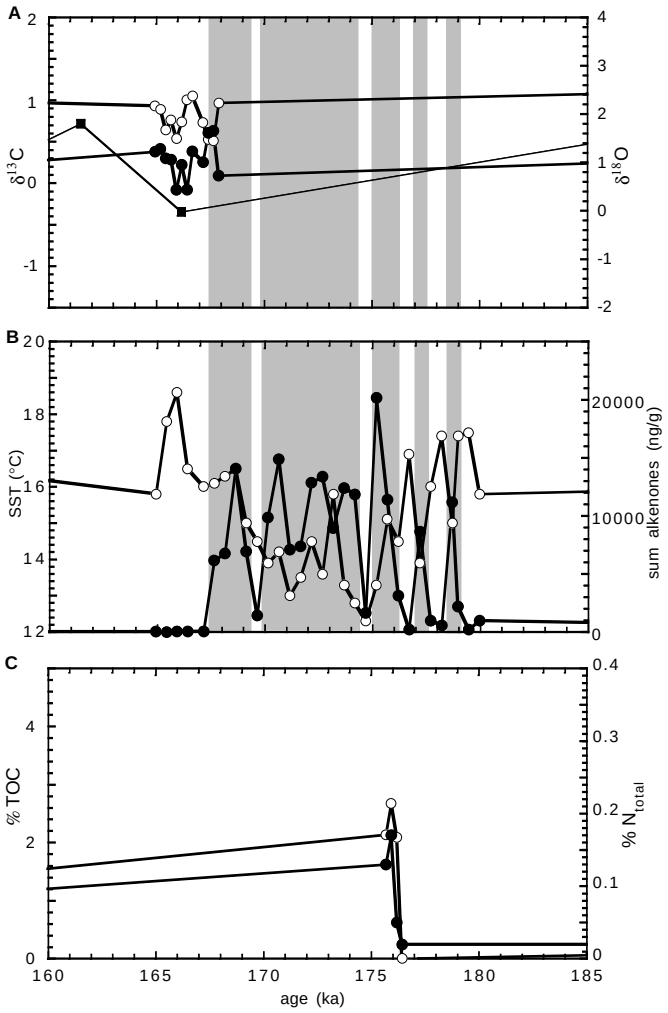

Figure 6. Plot of data for interval 160-967D-2H-1, 130 cm, to 2H-2, 42 cm. The depth interval of S6 is shaded and is disrupted by thin mud turbidites. Variables plotted as in Figure 5.

22°C and 24°C and cold sapropels, as those seen in the young group, have not been recognized.

DISCUSSION

To test some of the concepts relating the external (climatic variations) and internal (water-mass changes, productivity, and redox conditions) to sapropel formation, multi-proxy records were to be constructed from ODP Legs 160 and 161 materials along an east–west transect across the entire Mediterranean (Emeis, Robertson, Richter, et al., 1996; Comas, Zahn, Klaus, et al., 1996). It was expected that such a transect would allow us to synoptically map the hydrographic conditions throughout the Mediterranean at the sites of sapropel formation in the eastern and western basins.

A first portion of the temperature and salinity record for the eastern limb of a Mediterranean-wide transect was investigated here. The data of SST variations and stable carbon- and oxygen-isotope composition of planktonic foraminifers include Site 967, which is close to the Nile as a possible freshwater source, and the Ionian Basin Site 964, which documents an intermediate surface-water environment between the eastern and western basin, as well as a pelagic environment of considerable importance as a conduit for deep-water and surface inflow.

The SST and stable-isotope records represent hydrographic boundary conditions such as stability of the water column, temperature gradients indicative of upwelling, and salinity changes. They also highlight the general temperature history and thus the long-term climatic evolution of the Eastern Mediterranean Sea and adjoining land areas.

Sea-Surface Temperatures

Our data from locations in the Ionian and Levantine Basins contain information on two time scales about the evolution of SST in the Eastern Mediterranean. The individual sapropel layers are witnesses of a particular state of the Mediterranean Sea environment and of its hydrography in the surface layer. The variations of SST records over a long time period tell us how temperature in the Eastern Mediterranean behaved in relation to global climate. Each interval analyzed in high temporal resolution is a record of short-term (hundreds of years) variability in SST and salinities. If we further use the sapropel intervals as time markers and as well-defined time slices in the tempera-

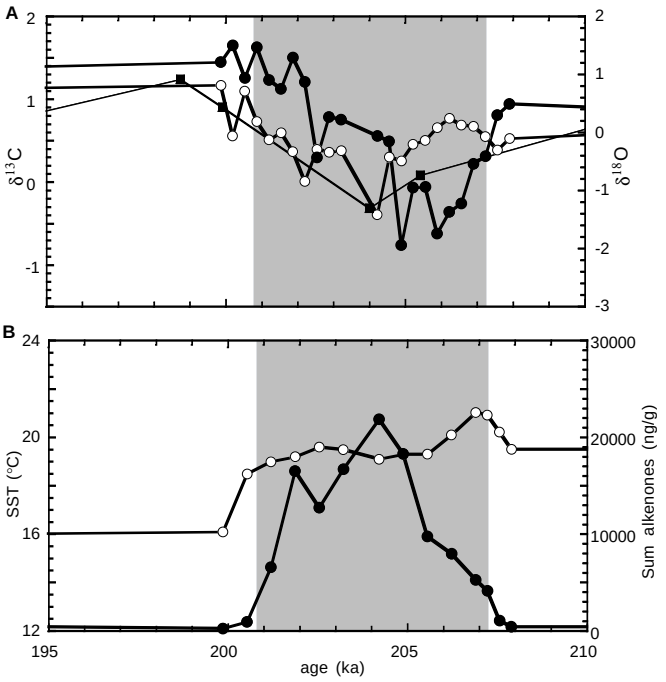

Figure 7. Plot of data for interval 160-967D-2H-2, 130 cm, to 2H-3, 4 cm. The depth interval of S7 is shaded. Variables plotted as in Figure 2.

ture history of the Mediterranean Sea, we may begin to reconstruct gradients in the thermal structure of the basin.

The sapropel records bear an imprint of external (insolation) and internal (baseline SST influenced by global/regional glaciation) forcing. Figure 26 is a plot that illustrates the average temperatures (and ±1σ standard deviations) of sapropel layers at the three core locations plotted against two types of climate records: (1) an ice-volume record (the benthic isotope record at Site 849 in the equatorial Pacific Ocean; Mix et al., 1995), and (2) a northern hemisphere insolation record (65°N; Laskar, 1990). Note that the sapropel ages are adjusted to precession minima as explained in Lourens et al. (1996) at this preliminary stage of our stratigraphic analyses. For most of the sapropels in the late Quaternary group (S1–S10), the average temperatures trace the $\delta^{18}O$/ice-volume record closely. All sapropels except S2, S6, and S8 occur during interglacial conditions, and temperatures are on average >17°C. Broadly speaking, maximal temperatures are found in sapropels that coincide with minimal interglacial ice volume paired with maximal northern hemisphere insolation. However, as has been shown before, SST and sapropel formation are not forced by global climate (Cita et al., 1977). Three of the late Quaternary sapropels were formed when high insolation coincided with glacial or weak interglacial conditions (S2, S6, and S8) and reflect this in low average temperatures. Insolation alone apparently does not determine the SST during sapropel formation, because the global background is still discernible and determines the temperature baseline: their average temperatures are significantly lower than those of the interglacial sapropels.

In older sapropels (Fig. 26), the pattern of cold and warm sapropels in accordance with the global ice-volume record is continued until ~650 ka. In those sapropels deposited from 900 to 1300 ka, the temperatures are more stable and are between 18°C and ~20°C. In the oldest sapropels (>2200 ka), the average temperatures are between 22°C and 24°C and appear to be unrelated to either insolation intensity or ice volume (Fig. 26C, 26D). However, the stratigraphy used for age assignment for these old sapropels is at present too poor and does not permit final statements.

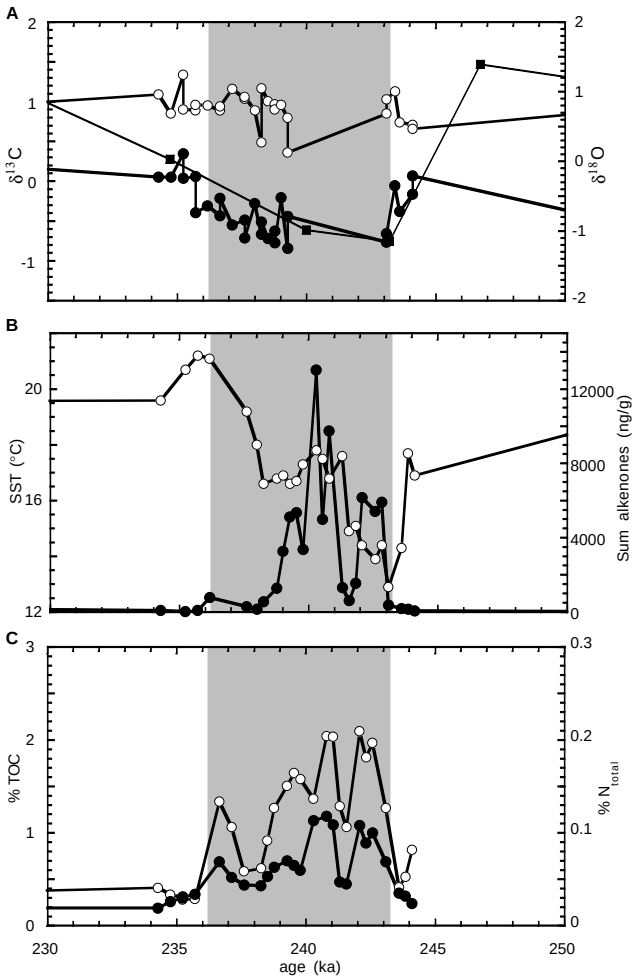

Figure 8. Plot of data for interval 160-967D-2H-3, 60–110 cm. The depth interval of S8 is shaded. Variables plotted as in Figure 5.

Temperature Gradients

The temperature gradients in coeval sapropels (Figs. 11, 26) do not substantiate the hypothesis of a circulation reversal as a cause for sapropel deposition. Upwelling of colder, nutrient-rich water, which would be one consequence of such a reversal, has been postulated as one possible consequence of a significant change in the e/p values (Calvert et al., 1992). Our combined records show no gradients in SST between the Levantine Basin Site 967 and the Ionian Basin Site 964/Core KC01 during the formation of sapropels. Today, the temperature gradient between the two locations is 2°C–3°C during the months of March and April, when the spring bloom occurs.

If an enrichment of nutrients in the eastern basin were caused by an inflow and Eastern Mediterranean ascent of subthermocline water from the adjoining Western Mediterranean Sea, the gradient should be reversed. Because increased nutrient concentrations in upwelling waters are inevitably associated with a shoaling of isotherms, upwelling areas are usually characterized by cool surface water. Within error margins of ±1σ, the temperatures at both locations covaried during all sapropel events since 350 ka, and temperatures in the eastern basin are equal to or slightly higher than in the central basin (Figs. 11, 26). An exception is S5, where the temperature profile in the sapropel deposited in the central basin (Core KC01) decreases by almost 5°C over the course of its deposition, whereas they increase by

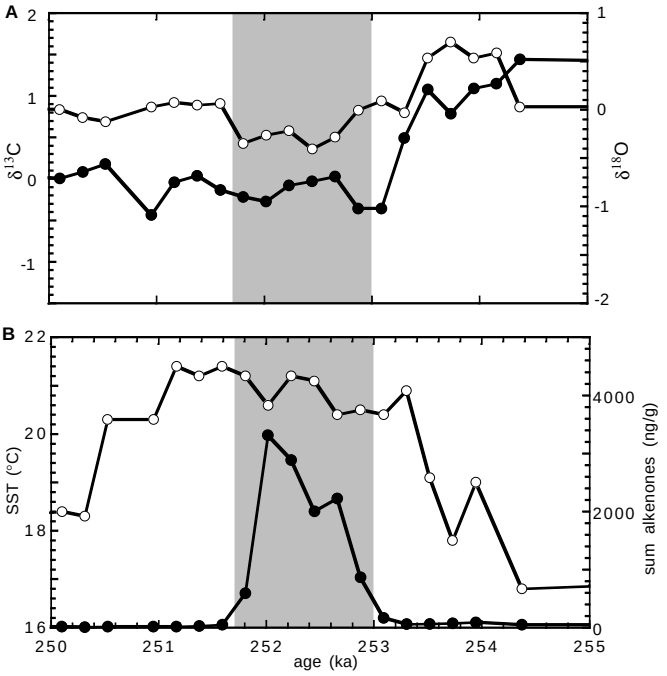

Figure 9. Plot of data for interval 160-967D-2H-3, 140 cm, to 2H-4, 10 cm. The depth interval of S9 is shaded. Variables plotted as in Figure 2.

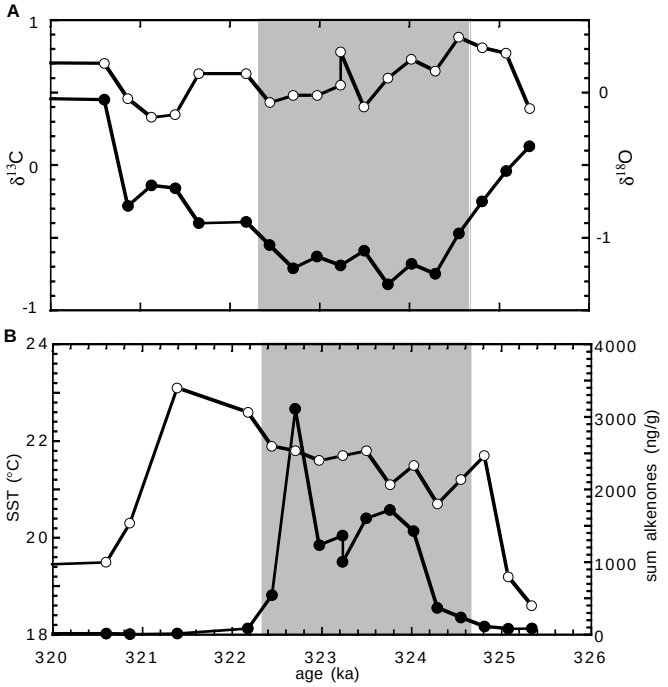

Figure 10. Plot of data for interval 160-967D-2H-5, 125–145 cm. The depth interval of S10 is shaded. Variables plotted as in Figure 2.

7°C in the Levant (Fig. 11C). In most cases, the average SST at Site 967 is slightly (but insignificantly) warmer than at Site 964/Core KC01 and may reflect the lag in SST warming during the course of spring from the southeast to the northwest. In the case of S9, the temperature at Site 967 is lower than that in Core KC01, but is not statistically different (Fig. 26).

Because we see changes in SST in the records both within and outside the actual sapropels, the reason for the lack of a gradient cannot be a mere response of the alkenone-producing phytoplankton to seasonal warming. For example, if the alkenone record were created during blooms starting when the photic zone is stabilized at its base by the 18°C isotherm, the temperature should always be 18°C, and we would get a flat curve. The data instead suggest a spatially homogeneous temperature in the surface layer that needs to be verified and explained in future work.

Salinity Changes

The study of temperature- and salinity-sensitive organisms, palynological assemblages in sapropels, and analyses of the stable isotope composition of planktonic foraminifer tests, document dramatic decreases in salinity and temperature variations associated with some sapropel periods. With the exception of the $\delta^{18}O$ of foraminifer calcite, however, these methods are not suitable for quantitative reconstructions. The $\delta^{18}O$ of foraminifer calcite is controlled by four variables: species-dependent vital effects, which can be circumnavigated by using one species of foraminifer, temperature changes, salinity changes, and the effect of changes in the inventory of light isotopes of oxygen in ice. To unravel the history of salinity changes and of sea-surface conditions that may have led to sapropel deposition, one must correct the $\delta^{18}O$ values planktonic foraminifer calcite for the effects of global ice volume and temperature.

Our next step towards clarifying the physical environment during sapropel formation is to attempt reconstructions of salinity, for which we use a combination of isotopic and temperature data. Table 3 shows a synthesis of the data from Table 1 and groups all observations that are relevant to estimates on how the surface conditions changed at Site 967 in the time before, during, and after a particular sapropel was deposited. Also given in Table 3 are estimates of the global ice volume (after Vogelsang, 1990), which are necessary to estimate the local salinity anomaly from $\delta^{18}O$ of planktonic foraminifers, alkenone sea-surface temperature estimates, and ice-volume estimates.

The following paragraph illustrates the procedures applied to calculate the changes in salinity for each of the sapropels. Sapropel S1 at Site 967 shows a gradual decrease of 1.9‰ in the $\delta^{18}O$ value from 1.2‰ below the sapropel to −0.66‰ within the sapropel. This change occurs over a period of ~1000 yr (Fig. 2A). During and after the sapropel event, the isotope composition remains fairly constant and varies around −0.1‰. The two extreme isotope values are accompanied by an increase in SST from 13.2°C to 18.7°C (Fig. 2B). To estimate the maximum salinity change associated with the sapropel, we use the data pair yielding the largest variation in $\delta^{18}O$ data below and within the sapropel. In Sapropel S1 at Site 967, this is the pair 1.21‰ (Sample 160-967D-1H-1, 135–136 cm) and −0.66‰ (Sample 160-967D-1H-1, 126–127 cm), which have SSTs of 13.2°C and 18.7°C (1 cm below), respectively. Using a temperature relationship of −0.2‰ $\delta^{18}O$ per 1°C means that up to −1.2‰ $\delta^{18}O$ is explained by temperature change. The residual −0.7‰ change toward lighter $\delta^{18}O$ values may be attributed to a combination in the effects of global ice-volume changes and local salinity changes. We use Vogelsang's (1990) estimate for the global ice effect for the time of S1 deposition to be 0.12‰ (at 8 ka), compared to 0.27‰ at 11 ka before the sapropel, amounting to a a global scale ice-effect amplitude of −0.15‰. This global portion subtracted from our residual leaves −0.55‰ [−0.70‰ −(−0.15‰)] as a local salinity signal. Using the relationship of 0.41‰ $\delta^{18}O$ per 1 psu (Thunell and Williams, 1989), the salinity decrease associated with Sapropel S1 at Site 967 was −1.5 (as a maximum value) in the Levantine Basin.

We performed the same calculation for all sapropels of the upper Pleistocene–Holocene group at Site 967 (Table 3). To estimate the

Table 2. Data for sapropels from Site 964.

Core, section, interval (cm)	Depth (mbsf)	Depth (rmcd)	Age (ka)	$\delta^{13}C$ (‰)	±1σ	$\delta^{18}O$ (‰)	±1σ	TC (%)	TN (%)	TIC (%)	TOC (%)	$U^{k'}_{37}$	SST (°C)	Σ alkenones (ng/g)
160-964E-														
2H-1, 97-98	6.47	12.56	231.5	0.57	0.02	0.22	0.04	4.1	0.1	3.8	0.4	0.685	19.0	22
2H-1, 98-99	6.48	12.58	231.9	0.68	0.01	0.22	0.02	3.8	0.1	3.6	0.2			
2H-1, 99-100	6.49	12.59	232.1	0.81	0.01	0.67	0.02	3.3	0.1	2.8	0.6	0.657	18.2	15
2H-1, 100-101	6.50	12.60	232.2	0.64	0.01	0.2	0.03	3.5	0.1	3.2	0.3			
2H-1, 101-102	6.51	12.61	232.4	0.61	0.02	0.34	0.03	3.8	0.1	3.5	0.3	0.615	16.9	5
2H-1, 102-103	6.52	12.63	232.7	–0.11	0.01	–0.17	0.02	3.5	0.1	3.1	0.4			
2H-1, 103-104	6.53	12.64	232.9	–0.04	0.03	–0.22	0.04	2.8	0.1	2.4	0.4	0.604	16.6	12
2H-1, 104-105	6.54	12.66	233.2	–0.23	0.02	–0.26	0.03	2.6	0.1	2.2	0.4			
2H-1, 105-106	6.55	12.67	233.4	0.29	0.01	0.21	0.03	2.8	0.1	2.3	0.4	0.580	15.9	36
2H-1, 106-107	6.56	12.69	233.7	0.13	0.01	–0.07	0.02	3.7	0.1	3.0	0.7			
2H-1, 107-108	6.57	12.70	233.9	0.63	0.01	–1.21	0.02	6.7	0.2	4.1	2.6	0.547	14.9	5,786
2H-1, 108-109	6.58	12.72	234.3					6.4	0.2	3.8	2.6			
2H-1, 109-110	6.59	12.73	234.4					6.2	0.2	3.4	2.7	0.536	14.6	5,954
2H-1, 110-111	6.60	12.75	234.8					6.6	0.2	3.8	2.8			
2H-1, 111-112	6.61	12.76	234.9					5.8	0.2	3.2	2.6	0.573	15.7	5,477
2H-1, 112-113	6.62	12.77	235.1					6.9	0.2	4.0	2.9			
2H-1, 113-114	6.63	12.78	235.3					6.8	0.2	4.3	2.6	0.591	16.2	4,132
2H-1, 114-115	6.64	12.79	235.4					6.8	0.2	4.4	2.4			
2H-1, 115-116	6.65	12.80	235.6					6.3	0.2	3.1	3.3	0.527	14.4	292
2H-1, 116-117	6.66	12.82	235.9					6.4	0.2	4.2	2.2			
2H-1, 117-118	6.67	12.83	236.1					6.2	0.2	3.9	2.3	0.502	13.6	1,934
2H-1, 118-119	6.68	12.84	236.3					5.7	0.2	3.6	2.1			
2H-1, 119-120	6.69	12.85	236.5					5.9	0.2	3.9	2.1	0.454	12.2	3,033
2H-1, 120-121	6.70	12.87	236.8					6.2	0.2	3.9	2.2			
2H-1, 121-122	6.71	12.88	237.0					6.0	0.2	3.5	2.4	0.473	12.8	2,815
2H-1, 122-123	6.72	12.89	237.1					5.6	0.2	3.5	2.2			
2H-1, 123-124	6.73	12.90	237.3	0.69	0.02	–1.19	0.04	4.5	0.1	3.2	1.3	0.486	13.1	808
2H-1, 124-125	6.74	12.92	237.6	0.60	0.02	–0.73	0.06	3.9	0.1	3.2	0.7			
2H-1, 125-126	6.75	12.93	237.8	0.85	0.02	–0.57	0.02	3.9	0.1	3.2	0.6	0.430	11.5	24
2H-1, 126-127	6.76	12.94	238.0	0.64	0.01	–0.24	0.04	3.9	0.1	3.4	0.5			
2H-1, 127-128	6.77	12.95	238.1	0.60	0.04	–0.39	0.02	4.0	0.1	3.4	0.6	0.444	11.9	36
2H-1, 128-129	6.78	12.96	238.3	0.41	0.03	–0.18	0.04	3.9	0.1	3.2	0.8			
2H-1, 129-130	6.79	12.97	238.5	0.49	0.03	–0.54	0.05	4.0	0.1	3.7	0.4	0.442	11.9	39
2H-1, 130-131	6.80	12.99	238.8	0.81	0.02	–0.10	0.03	3.7	0.1	3.1	0.6			
2H-1, 131-132	6.81	13.00	239.0	0.86	0.01	0.15	0.02	3.7	0.1	3.2	0.5	0.496	13.4	21
2H-2, 91-92	17.41	22.50	495.9					3.4	0.0	3.0	0.4	0.643	17.8	10
2H-2, 92-93	17.42	2.51	496.2					3.4	0.0	3.1	0.3			
2H-2, 93-94	17.43	2.52	496.6					3.5	0.0	3.1	0.3	0.637	17.6	9
2H-2, 94-95	17.44	2.53	496.9					3.6	0.0	3.2	0.4			
2H-2, 95-96	17.45	2.54	497.3					4.5	0.1	4.2	0.4	0.774	21.6	127
2H-2, 96-97	17.46	2.55	497.6	0.93	0.02	–0.08	0.01	6.2	0.1	5.6	0.6			
2H-2, 97-98	17.47	2.56	497.9					6.9	0.1	6.1	0.8	0.738	20.6	1,233
2H-2, 98-99	17.48	2.57	498.3	0.84	0.01	–0.36	0.01	8.5	0.2	5.8	2.7			
2H-2, 99-100	17.49	2.58	498.6					8.5	0.2	5.4	3.1	0.713	19.8	3,869
2H-2, 100-101	17.50	2.59	499.0	0.66	0.01	–0.26	0.03	8.2	0.2	4.9	3.3			
2H-2, 101-102	17.51	2.60	499.3					7.4	0.2	4.5	2.9	0.673	18.6	2,865
2H-2, 102-103	17.52	2.61	499.7	–2.62	0.02	–7.52	0.03	5.7	0.1	4.2	1.5			
2H-2, 103-104	17.53	2.62	500.1					4.6	0.1	3.9	0.7	0.717	20.0	444
2H-2, 104-105	17.54	2.63	500.5	1.33	0.02	–0.01	0.04	4.4	0.1	3.8	0.6			
2H-2, 105-106	17.55	2.64	500.9					4.5	0.1	4.0	0.5			
2H-2, 106-107	17.56	2.65	501.3	1.74	0.01	0.35	0.02	4.6	0.1	4.1	0.5			
2H-2, 107-108	17.57	2.66	501.7					4.4	0.1	3.8	0.6	0.579	15.9	35
2H-2, 108-109	17.58	2.67	502.2	1.13	0.02	1.29	0.03	4.4	0.1	3.9	0.5			
2H-2, 109-110	17.59	2.68	502.6					5.1	0.1	4.5	0.7	0.594	16.3	51
2H-3, 63-64	18.63	23.85	546.3	0.40	0.02	0.21	0.02	4.9	0.1	4.6	0.4	0.598	16.4	27
2H-3, 64-65	18.64	23.86	546.7					4.8	0.1	4.3	0.6			
2H-3, 65-66	18.65	23.87	547.1	0.67	0.02	–0.11	0.03	5.0	0.1	4.8	0.2	0.574	15.7	41
2H-3, 66-67	18.66	23.89	547.6					5.2	0.1	n.d.	n.d.			
2H-3, 67-68	18.67	23.90	548.0	0.24	0.01	–0.24	0.02	4.8	0.1	4.4	0.4	0.561	15.4	74
2H-3, 68-69	18.68	23.91	548.4					4.9	0.1	4.4	0.5			
2H-3, 69-70	18.69	23.92	548.9	0.43	0.02	–0.48	0.05	8.9	0.2	6.0	2.9	0.526	14.3	8,127
2H-3, 70-71	18.70	23.93	549.3					7.2	0.2	5.3	1.9			
2H-3, 71-72	18.71	23.94	549.7	0.37	0.02	–0.75	0.03	5.2	0.1	4.4	0.8	0.521	14.2	860
2H-3, 72-73	18.72	23.95	550.2					5.5	0.1	4.3	1.2			
2H-3, 73-74	18.73	23.96	550.6	0.62	0.02	–0.86	0.03	6.6	0.1	4.8	1.7	0.520	14.2	3,642
2h-3, 74-75	18.74	23.97	551.0					7.9	0.2	4.9	3.0			
2H-3, 75-76	18.75	23.98	551.4	0.27	0.02	–0.95	0.03	8.1	0.2	5.2	2.9	0.527	14.3	4,797
2H-3, 76-77	18.76	24.00	551.8					8.2	0.2	5.4	2.8			
2H-3, 77-78	18.77	24.01	552.2	0.26	0.02	–0.59	0.02	7.7	0.1	5.3	2.4	0.532	14.5	4,874
2H-3, 78-79	18.78	24.02	552.6					7.7	0.2	4.9	2.8			
2H-3, 79-80	18.79	24.03	553.0	0.63	0.02	–1.25	0.05	7.7	0.2	4.8	2.9	0.567	15.5	4,522
2H-3, 80-81	18.80	24.04	553.4					5.6	0.1	4.2	1.4			
2H-3, 81-82	18.81	24.05	553.7	0.29	0.01	–0.55	0.02	5.0	0.1	4.1	0.9	0.572	15.7	948
2H-3, 82-83	18.82	24.06	554.1					3.9	0.0	3.3	0.5			
2H-3, 83-84	18.83	24.07	554.5	1.01	0.02	1.11	0.04	3.8	0.0	3.2	0.6	0.498	13.5	99
2H-3, 84-85	18.84	24.08	554.9					3.8	0.0	3.3	0.5			
2H-3, 85-86	18.85	24.09	555.2	1.07	0.01	1.28	0.04	4.2	0.0	n.d.	n.d.	0.438	11.7	66
2H-3, 86-87	18.86	24.10	555.6					5.0	0.0	3.7	1.3			
2H-3, 87-88	18.87	24.11	556.0	1.01	0.02	1.07	0.03	5.3	0.0	4.8	0.5	0.485	13.1	112
2H-4, 44-45	19.94	25.20	599.3	1.42	0.02	1.26	0.05	5.1	0.0	4.4	0.7			
2H-4, 45-46	19.95	25.21	599.7					4.7	0.0	4.4	0.3	0.553	15.1	8
2H-4, 46-47	19.96	25.2	600.5	1.33	0.02	1.11	0.04							
2H-4, 47-48	19.97	25.23	600.6	1.31	0.02	0.40	0.01	2.4	0.1	2.2	0.2	0.670	18.6	37
2H-4, 48-49	19.98	25.24	601.0	1.30	0.02	1.29	0.01	6.5	0.0	6.2	0.3			
2H-4, 49-50	19.99	25.25	601.4	1.28	0.02	0.80	0.03	2.5	0.1	2.1	0.4	0.691	19.2	118
2H-4, 54-55	20.05	25.28	604.1	1.66	0.01	0.74	0.02	5.7	0.0	5.3	0.3			
2H-4, 55-56	20.05	25.31	604.1	1.13	0.01	0.17	0.03	5.8	0.0	5.2	0.6	0.635	17.5	44
2H-4, 56-57	20.06	25.33	604.5	0.84	0.01	–0.25	0.03	6.0	0.0	5.7	0.3			
2H-4, 57-58	20.07	25.34	605.0	1.02	0.01	–0.42	0.02	6.2	0.0	5.6	0.6	0.595	16.4	87

Table 2 (continued).

Core, section, interval (cm)	Depth (mbsf)	Depth (rmcd)	Age (ka)	$\delta^{13}C$ (‰)	±1σ	$\delta^{18}O$ (‰)	±1σ	TC (%)	TN (%)	TIC (%)	TOC (%)	$U^{k'}_{37}$	SST (°C)	Σ alkenones (ng/g)
				0.72	0.02	–0.73	0.04							
2H-4, 78-79	20.28	25.56	614.3	0.25	0.01	–0.58	0.03	7.2	0.0	6.9	0.3			
2H-4, 79-80	20.29	25.57	614.7	0.29	0.02	–0.35	0.03	6.8	0.0	6.6	0.3	0.624	17.2	47
2H-4, 81-82	20.31	25.59	615.6	1.43	0.01	0.73	0.04	6.5	0.0	6.2	0.3	0.434	11.6	56
2H-4, 82-83	20.31	25.62	615.6	0.66	0.02	–2.11	0.03	5.3	0.0	4.9	0.4			
2H-4, 87-88	20.37	25.65	618.0	0.38	0.01	–2.2	0.01	4.9	0.1	4.5	0.4	0.713	19.8	45
2H-4, 98-99	20.48	25.70	622.0	0.73	0.02	–1.30	0.04	5.1	0.0	4.4	0.7			
2H-4, 99-100	20.49	25.75	622.5	0.98	0.01	0.23	0.02	4.7	0.0	4.2	0.5	0.605	16.6	119
2H-4, 100-101	20.49	25.76	622.5					4.6	0.1	4.1	0.5			
160-964D-														
4H-4, 105-106	28.65	34.09	972.3	1.33	0.02	0.26	0.02		0.2		2.4	0.936	26.4	25
4H-4, 107-108	28.67	34.11	973.2	1.21	0.02	0.28	0.01		0.3		2.6	0.983	27.8	18
4H-4, 109-110	28.69	34.13	974.0	1.36	0.03	–0.12	0.03		0.2		2.1			
4H-4, 111-112	28.71	34.15	974.8	1.02	0.02	–0.24	0.04		0.2		1.9	0.953	26.9	52
4H-4, 113-114	28.73	34.17	975.6	0.78	0.01	0.13	0.02		0.0		0.2			
4H-4, 115-116	28.75	34.19	976.5						0.1		0.3			
4H-4, 117-118	28.77	34.21	977.3						0.1		3.4	0.790	22.1	134
4H-4, 119-120	28.79	34.23	978.1	0.74	0.02	0.70	0.05		0.0		0.4			
4H-4, 121-12	28.81	34.25	979.0	0.83	0.02	–0.37	0.02		0.2		1.8			
4H-4, 123-124	28.83	34.27	979.8	0.97	0.01	0.94	0.02		0.2		1.9			
4H-4, 125-126	28.85	34.29	980.6						0.1		0.9	0.602	16.6	153
4H-4, 127-128	28.87	34.31	981.5	1.36	0.01	–0.63	0.02		0.0		0.2			
4H-4, 129-130	28.89	34.33	982.3						0.0		0.6	0.839	23.5	25
4H-4, 131-132	28.91	34.35	983.1	1.77	0.01	–0.66	0.03		0.0		0.5			
4H-5, 23-24	29.33	34.77	1000.6									0.665	18.4	98
4H-5, 25-25	29.35	34.79	1001.4									0.540	14.7	242
				1.10	0.01	–0.48	0.02							
4H-5, 61-62	29.71	35.15	1016.4						0.0		0.1	0.749	20.9	
4H-5, 62-63	29.72	35.16	1016.9	0.92	0.03	–0.43	0.02							
4H-5, 63-64	29.73	35.17	1017.3						0.0		0.1	0.813	22.8	
4H-5, 64-65	29.74	35.18	1017.7	0.60	0.02	–0.31	0.04							
4H-5, 65-66	29.75	35.19	1018.1						0.1		0.3	0.746	20.8	
4H-5, 66-67	29.76	35.20	1018.6											
4H-5, 67-68	29.77	35.21	1019.0						0.1		2.2	0.692	19.2	
4H-5, 68-69	29.78	35.2	1019.4	0.81	0.03	–0.81	0.04							
4H-5, 69-70	29.79	35.23	1019.8						0.0		0.8	0.715	19.9	
4H-5, 70-71	29.80	35.24	1020.2	1.45	0.02	–0.22	0.03							
4H-5, 71-72	29.81	35.25	1020.6						0.0		0.3	0.609	16.8	
4H-5, 72-73	29.82	35.26	1021.1											
4H-5, 73-74	29.83	35.27	1021.5						0.0		0.2			
4H-5, 74-75	29.84	35.28	1021.9											
4H-5, 75-76	29.85	35.29	1022.3						0.0		0.2	0.735	20.5	
4H-5, 76-77	29.86	35.30	1022.8	0.87	0.02	0.85	0.07							
4H-5, 77-78	29.87	35.31	1023.2						0.0		0.2	0.539	14.7	
4H-5, 78-79	29.88	35.32	1023.6	1.35	0.02	1.39	0.02							
4H-5, 79-80	29.89	35.33	1024.0						0.0		0.2	0.498	13.5	
4H-5, 134-135	30.44	35.88	1047.1	1.10	0.03	0.44	0.04					0.700	19.4	8
4H-5, 135-136	30.45	35.89	1047.6						0.0		0.1			
4H-5, 136-137	30.46	35.90	1048.0	1.30	0.04	0.23	0.04					0.632	17.4	14
4H-5, 137-138	30.47	35.91	1048.4						0.0		0.1			
4H-5, 138-139	30.48	35.92	1048.8	1.59	0.02	0.84	0.03					0.627	17.3	4
4H-5, 139-140	30.49	35.93	1049.2						0.1		0.2			
4H-5, 140-141	30.50	35.94	1049.7									0.726	20.2	577
4H-5, 141-142	30.51	35.95	1050.1						0.2		4.4			
4H-5, 142-143	30.52	35.96	1050.5									0.738	20.6	5,267
4H-5, 143-144	30.53	35.97	1050.9						0.1		3.0			
4H-5, 144-145	30.54	35.98	1051.4	1.02	0.01	–0.95	0.02					0.676	18.7	5,485
4H-5, 145-146	30.55	35.99	1051.8						0.1		1.8			
4H-5, 146-147	30.56	36.00	1052.2	1.18	0.02	–0.42	0.04					0.579	15.9	670
4H-5, 147-148	30.57	36.01	1052.6						0.1		1.0			
4H-5, 148-149	30.58	36.02	1053.0	1.08	0.01	0.39	0.03					0.587	16.1	186
4H-5, 149-150	30.59	36.03	1053.5						0.0		0.4			
4H-5, 150-151	30.60	36.04	1053.9	1.10	0.02	0.82	0.05					0.569	15.6	36
4H-6, 80-81	31.40	36.84	1087.5	1.70	0.01	0.58	0.02					0.725	20.2	14
4H-6, 81-82	31.41	36.85	1087.9						0.0		0.2			
4H-6, 82-83	31.42	36.86	1088.3	1.39	0.01	0.62	0.01					0.675	18.7	28
4H-6, 83-84	31.43	36.87	1088.7						0.0		0.1			
4H-6, 84-85	31.44	36.88	1089.2	1.31	0.01	0.24	0.05					0.695	19.3	12
4H-6, 85-86	31.45	36.89	1089.6						0.0		0.1			
4H-6, 86-87	31.46	36.90	1090.0									0.676	18.7	33
4H-6, 87-88	31.47	36.91	1090.4						0.0		0.2			
4H-6, 88-89	31.48	36.92	1090.8	0.90	0.01	0.34	0.03					0.724	20.1	20
4H-6, 89-90	31.49	36.93	1091.3						0.0		0.2			
4H-6, 90-91	31.50	36.94	1091.7	0.87	0.01	0.48	0.03					0.822	23.0	105
4H-6, 91-92	31.51	36.95	1092.1						0.1		0.3			
4H-6, 92-93	31.52	36.96	1092.5									0.752	21.0	45,227
4H-6, 93-94	31.53	36.97	1092.9						0.4		9.0			
4H-6, 94-95	31.54	36.98	1093.4									0.687	19.1	17,923
4H-6, 95-96	31.55	36.99	1093.8						0.3		7.2			
4H-6, 96-97	31.56	37.00	1094.2									0.679	18.8	8,421
4H-6, 97-98	31.57	37.01	1094.6						0.0		2.6			
4H-6, 98-99	31.58	37.02	1095.0	1.69	0.02	–0.60	0.02					0.671	18.6	133
4H-6, 99-100	31.59	37.03	1095.5						0.0		1.4			
4H-6, 100-101	31.60	37.04	1095.9	1.50	0.02	0.37	0.03					0.678	18.8	36
4H-6, 101-102	31.61	37.05	1096.3						0.0		0.5			
4H-6, 102-103	31.62	37.06	1096.7	1.70	0.01	0.30	0.02							
4H-6, 103-104	31.63	37.07	1097.1						0.0		0.3			
4H-6, 104-105	31.64	37.08	1097.6	1.47	0.02	0.33	0.01					0.734	20.5	28
4H-6, 105-106	31.65	37.09	1098.0						0.0		0.2			
4H-7, 25-26	32.35	37.77	1126.5	1.39	0.01	0.43	0.03		0.0		0.3			
4H-7, 27-28	32.37	37.79	1127.4	1.23	0.01	0.92	0.03		0.0		0.2			

Table 2 (continued).

Core, section, interval (cm)	Depth (mbsf)	Depth (rmcd)	Age (ka)	$\delta^{13}C$ (‰)	±1σ	$\delta^{18}O$ (‰)	±1σ	TC (%)	TN (%)	TIC (%)	TOC (%)	$U^{k'}_{37}$	SST (°C)	Σ alkenones (ng/g)
4H-7, 29-30	32.39	37.80	1127.8	1.39	0.02	0.42	0.03		0.0		0.1			
4H-7, 31-32	32.41	37.82	1128.6	0.91	0.02	0.49	0.04		0.1		0.2			
4H-7, 33-34	32.43	37.84	1129.5						0.2		3.9	0.692	19.2	1,903
4H-7, 35-36	32.45	37.86	1130.3						0.1		3.4	0.706	19.6	26,156
4H-7, 37-38	32.47	37.88	1131.1	0.33	0.02	–1.14	0.03		0.1		2.5	0.754	21.0	9,997
4H-7, 39-40	32.49	37.90	1132.0	0.81	0.03	–0.78	0.04		0.0		0.7	0.569	15.6	204
4H-7, 41-42	32.51	37.91	1132.4	0.54	0.02	–0.11	0.02		0.0		0.4	0.638	17.6	29
4H-7, 43-44	32.53	37.92	1132.8	0.38	0.03	–0.13	0.04		0.0		0.3	0.586	16.1	36
4H-7, 45-46	32.55	39.93	1217.2	0.49	0.02	0.18	0.03		0.0		0.2	0.548	15.0	30
5H-2, 75-76	34.85	41.67	1279.1	0.60	0.03	–0.38	0.04		0.0		0.1	0.648	17.9	9
5H-2, 77-78	34.87	41.69	1279.7	0.57	0.02	–0.38	0.02		0.0		0.1	0.752	21.0	8
5H-2, 79-80	34.89	41.71	1280.3	0.79	0.03	–0.49	0.01		0.0		0.2	0.679	18.8	30
5H-2, 81-82	34.91	41.73	1280.9						0.1		1.2	0.690	19.1	2,973
5H-2, 83-84	34.93	41.75	1281.5	0.49	0.01	–0.86	0.02		0.2		3.8	0.611	16.8	1,740
5H-2, 85-86	34.95	41.77	1282.2	0.84	0.03	–0.76	0.05		0.1		1.8	0.628	17.3	848
5H-2, 87-88	34.97	41.79	1282.8	0.51	0.03	–0.45	0.05		0.0		0.3	0.690	19.1	80
5H-2, 89-90	34.99	41.81	1283.4	0.26	0.01	–0.69	0.04					0.625	17.2	935
5H-2, 91-92	35.01	41.83	1284.0	1.36	0.01	0.29	0.04					0.569	15.6	60
5H-2, 93-94	35.03	41.85	1284.6	0.84	0.02	0.34	0.03					0.586	16.1	29
5H-2, 95-96	35.05	41.87	1285.2	1.35	0.04	1.31	0.04					0.491	13.3	37
5H-2, 97-98	35.07	41.89	1285.8	1.28	0.02	0.99	0.04					0.553	15.1	34
5H-2, 99-100	35.08	41.91	1286.4	0.93	0.02	0.95	0.05							
160-964E-														
4H-2, 14-15	58.64	74.02	2275.4					7.4	0.0	6.8	0.5	0.831	23.3	25
4H-2, 16-17	58.66	74.04	2275.8					7.3	0.0	6.8	0.5			
4H-2, 18-19	58.68	74.06	2276.2					7.5	0.0	7.2	0.3	0.811	22.7	469
4H-2, 20-21	58.70	74.09	2276.9	0.75	0.01	0.09	0.02	7.6	0.0	6.7	0.9	0.883	24.8	824
4H-2, 2-23	58.72	74.11	2277.3	0.51	0.02	–1.01	0.05	7.7	0.1	6.3	1.4	0.810	22.7	1,154
4H-2, 24-25	58.74	74.13	2277.7	0.54	0.02	–0.63	0.04	7.7	0.1	6.2	1.5	0.817	22.9	849
4H-2, 26-27	58.76	74.15	2278.1	0.79	0.03	–0.19	0.05	7.7	0.1	6.6	1.1	0.788	22.0	1,070
4H-2, 28-29	58.78	74.17	2278.5	1.06	0.03	–0.10	0.07	7.8	0.1	6.3	1.5	0.802	22.4	166
4H-2, 30-31	58.80	74.19	2278.9					7.1	0.0	6.1	1.0	0.812	22.7	340
4H-2, 32h-33	63.32	74.21	2279.3	1.37	0.03	–0.20	0.03	7.9	0.1	6.0	1.8	0.829	23.2	2,463
4H-2, 34-35	58.84	74.23	2279.7					8.1	0.1	5.7	2.3	0.828	23.2	109
4H-2, 36-37	58.86	74.25	2280.1					7.5	0.2	4.4	3.1	0.819	22.9	8,696
4H-2, 38-39	58.88	74.28	2280.7					11.9	0.4	5.1	6.8	0.809	22.6	30,697
4H-2, 40-41	58.90	74.30	2281.1	0.96	0.01	–0.63	0.03	9.0	0.2	6.6	2.4	0.787	22.0	4,646
4H-2, 42-43	58.92	74.32	2281.5	0.81	0.04	0.32	0.05	7.6	0.1	6.7	0.9	0.800	22.4	275
4H-2, 44-45	58.94	74.34	2281.9	0.84	0.02	–0.11	0.06	8.0	0.1	6.7	1.2	0.72	20.1	361
4H-2, 46-47	58.96	74.36	2282.3	1.30	0.03	–0.56	0.04	8.1	0.0	7.3	0.8	0.648	17.9	27
4H-2, 130-131	59.80	75.29	2301.3	1.80	0.02	–0.56	0.02	9.4	0.0	8.5	0.9	0.715	19.9	42
4H-2, 132-133	59.82	75.31	2301.7	1.37	0.01	0.04	0.01	8.9	0.0	8.6	0.3	0.746	20.8	48
4H-2, 134-135	59.84	75.33	2302.1	1.03	0.01	–0.41	0.03	8.5	0.1	8.1	0.4	0.808	22.6	125
4H-2, 136-137	59.86	75.36	2302.7	1.32	0.01	–0.59	0.02	8.4	0.0	8.1	0.3	0.776	21.7	34
4H-2, 138-139	59.88	75.38	2303.1	0.93	0.02	–0.42	0.03	7.5	0.1	7.1	0.4	0.818	22.9	87
4H-2, 140-141	59.90	75.40	2303.5					21.0	1.0	0.0	21.0	0.841	23.6	111,492
4H-2, 142-143	59.92	75.42	2303.9					18.5	0.8	1.5	17.0	0.827	23.2	92,552
4H-2, 144-145	59.94	75.44	2304.3					13.8	0.6	1.9	11.9	0.848	23.8	64,817
4H-2, 146-147	59.96	75.45	2304.5	0.77	0.03	–0.89	0.04	10.9	0.4	3.4	7.4	0.842	23.6	36,142
4H-2, 148-149	59.98	75.47	2304.9	1.10	0.03	–0.96	0.05	7.8	0.2	4.8	3.1	0.803	22.5	13,363
4H-3, 0-1	60.00	75.49	2305.3	1.01	0.03	–0.65	0.07	7.4	0.0	6.7	0.7	0.755	21.0	110
4H-3, 2-3	60.02	75.51	2305.8	1.03	0.02	–0.31	0.04	7.6	0.0	5.9	1.6	0.782	21.9	55
4H-3, 4-5	60.04	75.52	2306.0	0.83	0.02	–0.48	0.06	7.5	0.0	7.1	0.4	0.814	22.8	89
4H-3, 6-7	60.06	75.54	2306.4	0.79	0.02	–0.34	0.02	6.3	0.0	5.7	0.6	0.784	21.9	1,609
4H-3, 8-9	60.08	75.56	2306.8	0.91	0.02	–0.75	0.04	6.4	0.3	1.6	4.8	0.716	19.9	5,911
4H-3, 10-11	60.10	75.58	2307.2	0.76	0.03	0.00	0.03	6.0	0.1	4.2	1.8	0.743	20.7	4,669
4H-3, 12-13	60.12	75.61	2307.8	0.95	0.02	–1.42	0.02	5.1	0.0	4.6	0.5	0.673	18.7	76
4H-3, 14-15	60.14	75.63	2308.2	0.81	0.02	–1.19	0.04	5.5	0.0	4.9	0.7	0.653	18.1	36
5H-5, 82-83	73.32	92.02	2675.5	1.13	0.02	–0.13	0.05	6.8	0.0	6.3	0.5	0.797	22.3	17
5H-5, 84-85	73.34	92.04	2676.0	1.16	0.02	–0.46	0.03	5.8	0.0	5.1	0.6	0.773	21.6	38
5H-5, 86-87	73.36	92.07	2676.6	1.38	0.02	–0.12	0.01	1.4	0.1	0.9	0.5	0.810	22.7	35
5H-5, 88-89	73.38	92.10	2677.3	0.99	0.02	0.07	0.03	2.7	0.0	2.2	0.5	0.802	22.4	58
5H-5, 90-91	73.40	92.13	2678.0					3.2	0.0	2.5	0.7	0.804	22.5	125
5H-5, 92-93	73.42	92.15	2678.4	1.32	0.02	–0.09	0.03	7.6	0.2	3.9	3.7	0.853	23.9	24,480
5H-5, 94-95	73.44	92.18	2679.1					11.6	0.2	6.9	4.7	0.841	23.6	30,050
5H-5, 96-97	73.46	92.21	2679.8	1.47	0.01	0.25	0.02	10.2	0.1	7.0	3.2	0.794	22.2	12,474
5H-5, 98-99	73.48	92.23	2680.3	1.47	0.02	0.15	0.03	7.7	0.0	6.9	0.8	0.771	21.5	1,590
5H-5, 100-101	73.50	92.26	2680.9					7.6	0.0	6.9	0.7	0.864	24.3	1,240
5H-5, 102-103	73.52	92.28	2681.4	1.11	0.02	0.04	0.05	7.7	0.0	6.7	1.0	0.837	23.5	1,295
6H-2, 25-26	77.75	98.10	2813.7	0.02	-0.20	0.04		8.1	0.0	7.9	0.1			
6H-2, 27-28	77.77	98.12	2814.1	0.01	-0.03	0.02		8.0	0.0	8.2	0.0	0.764	21.3	28
6H-2, 29-30	77.79	98.14	2814.6	0.02	-0.20	0.03		7.8	0.0	7.7	0.1	0.718	20.0	9
6H-2, 31-32	77.81	98.17	2815.2	0.02	-0.09	0.02		5.3	0.1	5.0	0.3			
6H-2, 33-34	77.83	98.19	2815.7	0.03	-0.26	0.04		10.4	0.5	3.3	7.1	0.826	23.1	14,181
6H-2, 35-36	77.85	98.21	2816.2	0.02	-0.05	0.02		8.8	0.0	8.5	0.3	0.805	2.5	30
6H-2, 37-38	77.87	98.23	2816.6	0.02	0.13	0.03		9.2	0.1	9.0	0.3	0.833	23.4	27
6H-2, 39-40	77.89	98.26	2817.3	0.01	-0.12	0.03		9.5	0.0	9.4	0.1			
6H-2, 125-127	78.75	99.20	2845.4	0.01	-0.20	0.02						0.863	24.2	15
6H-2, 127-128	78.77	99.2	2846.0	0.36	2.01	0.37						0.843	23.6	21
6H-2, 129-130	78.79	99.25	2846.9	0.02	-0.06	0.03						0.888	25.0	9
6H-2, 131-132	78.81	99.27	2847.5	0.45	2.19	0.48						0.822	23.0	847
6H-2, 133-134	78.83	99.29	2848.1									0.768	21.4	14,514
6H-2, 135-136	78.85	99.31	2848.7									0.900	25.3	2,986
6H-2, 137-138	78.87	99.33	2849.3	0.02	-0.08	0.05						0.824	23.1	139
6H-2, 139-140	78.89	99.35	2849.9	0.03	-0.01	0.05						0.875	24.6	65
6H-2, 141-142	78.91	99.37	2850.5	0.02	0.09	0.04						0.862	24.2	410
6H-2, 143-144	78.93	99.39	2851.1	0.01	-0.52	0.02						0.832	23.3	328

Note: All abbreviations as in Table 1. Gray-shaded cells indicate samples with <20 foraminifer tests for isotope analyses.

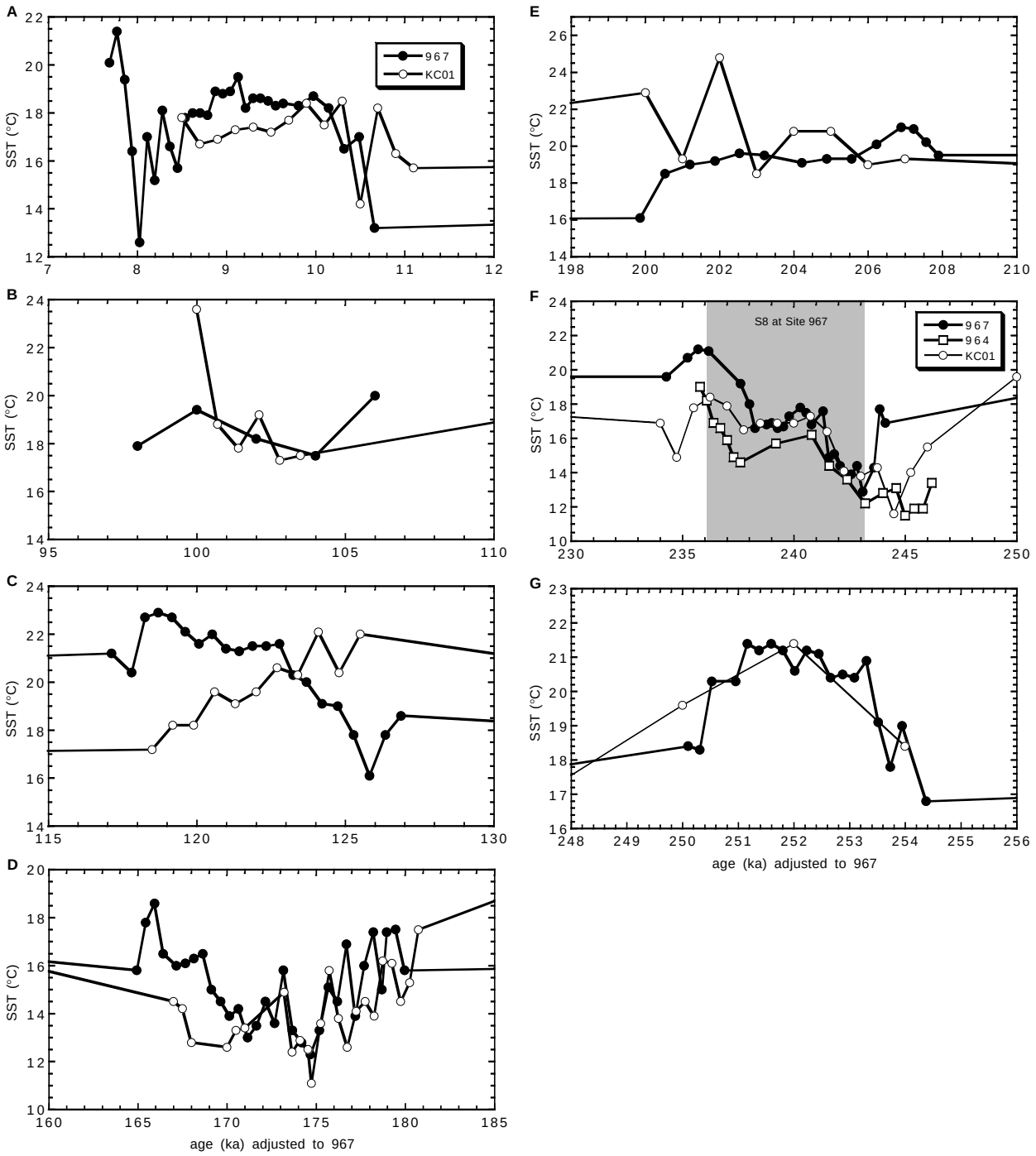

Figure 11. Comparison of SSTs for sapropels from Site 967 and Cores KC01/01B. Note that ages have been adjusted to fit the age estimates of Site 967 sapropels. **A.** S1. **B.** S4. **C.** S5. **D.** S6. **E.** S7. **F.** SST in S8 from three locations. **G.** S9. See text for discussion.

salinity change for each of the ten organic-rich layers, we use those data triplets ($\delta^{18}O$, SST, and ice-volume estimates) associated with sample pairs that yield the largest isotopic difference below and within the sapropels as extremes in the salinity change. Averaging over the entire duration of sapropel deposition and presapropel samples yields much more attenuated values, because these averages do not necessarily account for the range of change in salinity and temperature associated with the sapropels (Figs. 2A–10A). The reason is that each sapropel has a distinct signature, and the variables fluctuate considerably over time within the organic-carbon–rich layer. The fact that the proxies of salinity and temperature vary greatly within the sapropels is an indication that the environment during sapropel deposition was far from stable or uniform, but instead evolved during the time the sapropel was deposited.

In terms of salinity change, all sapropels coincide with decreases in surface salinities that range from 1.1 to 7.7 psu (Table 3). Most dramatic are the decreases for Sapropels S2, S4, and S7 (7.4, 7.7, and 6.2 psu, respectively). In all three cases, the temperatures do not increase from below to within the sapropels. SST remain constant (S2, S7) or even decrease (S4), while at the same time the $\delta^{18}O$ values show very large excursions to lighter values (S2 = –3.43‰; S4 = –2.94‰; S7 = –2.43‰).

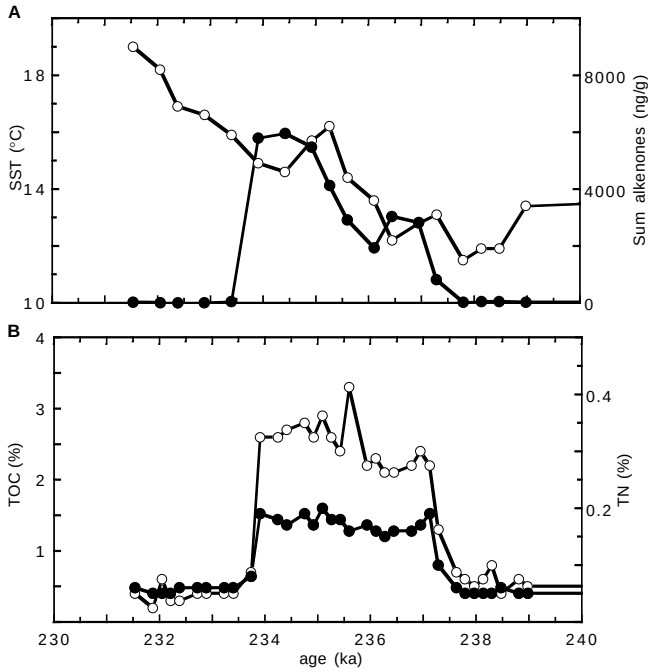

Figure 12. Plot of data for interval 160-964E-2H-1, 97–132 cm. **A.** Sea-surface temperature estimates from $U^{k'}_{37}$ values (open circles) and concentration of alkenones (filled circles; ng/g sediment). The alkenone concentrations indicate the extent of the organic-rich sapropel layer, as can be seen by comparison with **B.** Organic carbon concentrations (open circles) and total nitrogen concentrations (filled circles).

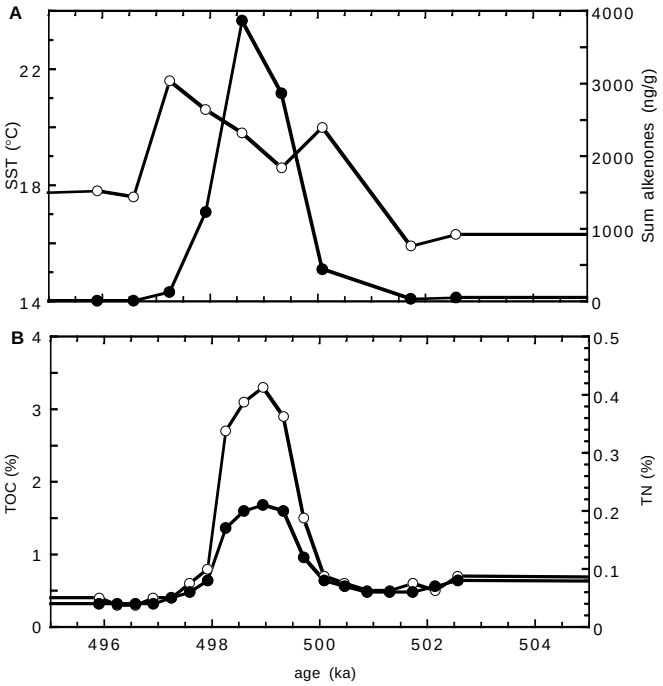

Figure 13. Plot of data for interval 160-964E-3H-2, 91–110 cm. Variables as in Figure 12.

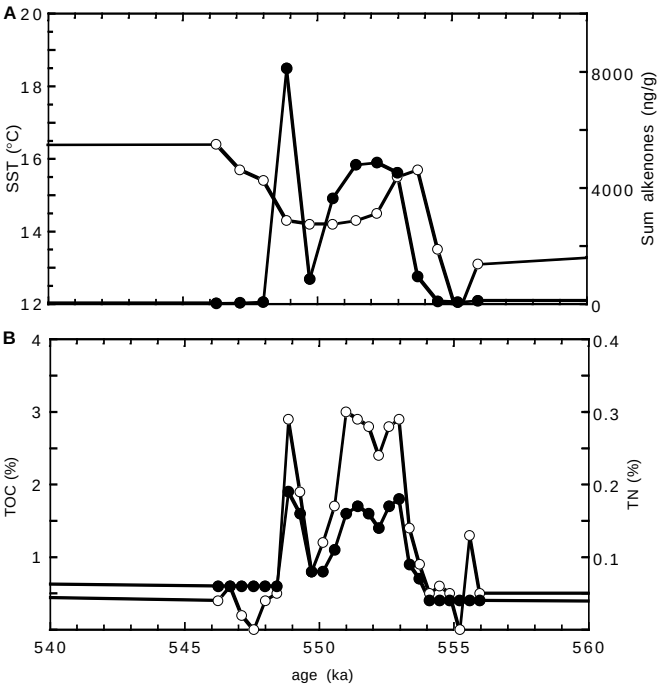

Figure 14. Plot of data for interval 160-964E-3H-3, 63–88 cm. Variables as in Figure 12.

Our salinity data for the Levantine Basin show that the water column has been much more stable during sapropel deposition than it is at present. It can be assumed that the salinity in the sea surface was similar to or higher than at present before each sapropel event in the past, because the present situation corresponds to an almost optimal climatic range (Béthoux 1993). This means that the subthermocline waters may have been either similar in density or even denser before each sapropel formed. The key to stable stratification (and inhibition of intermediate- and deep-water formation) is the density contrast between the surface mixed layer and the deeper waters. Only if temperature decreases or salinity increases to make surface waters sufficiently dense, will it sink to the level where it is stable within the density gradient of the water column. Today, the formation of intermediate-water masses is related to salinity increase of the Levantine Intermediate Water, which provides oxygen to water-depth intervals of 200–1500 m (Wüst, 1961). Formation of deep water occurs when winter cooling makes relatively fresh waters of the Liguran Sea and the Gulf of Lyons, the Adriatic, and the Aegean or Cretan Sea so dense that it sinks or cascades to the basin floors. The density contrasts today are very small and differ only by 1–2 units of σ_t.

A diagram of temperature vs. salinity (T-S) superimposed on lines of equal density σ_t, is shown in Figure 27. Because we have no means to determine the absolute salinity level before the onset of sapropel deposition from our data, we assume that each sapropel starts with a salinity of 39.08, which is typical for surface waters in the summer in the Levantine Sea today (Miller et al., 1970). The plot shows the measured SST and the assumed salinity of 39.08 for samples below sapropels (open circles) and SST and salinity values (39.08 ΔS from Table 3) for sapropels (solid circles). The field of T-S for the modern eastern Levantine Intermediate Water at 1500 m (gray area) is also indicated (Miller et al., 1970). The figure suggests that each sapropel analyzed from Site 967 has been accompanied by a surface-layer decrease in σ_t. of at least one unit and mostly of two or more units.

A simultaneous increase in SST coupled with a decrease in S, as is indicated for all sapropels, would result in a much more stable stratification of the upper-water column as that of today. This is an important further indication that sapropels formed during periods when reduced or inhibited intermediate- and deep-water formation led to a lack of oxygen recharge below the halocline. So far, our

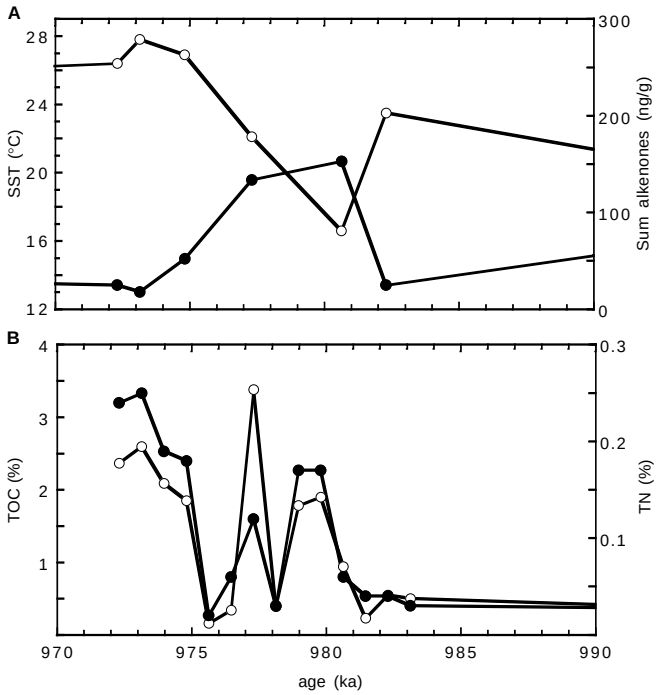

Figure 15. Plot of data for interval 160-964D-4H-4, 105–132 cm. Variables as in Figure 12.

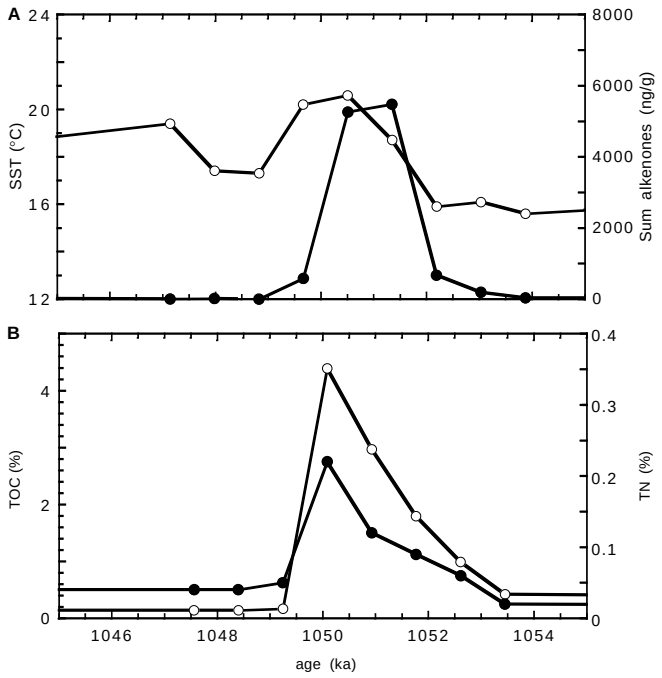

Figure 17. Plot of data for interval 160-964D-4H-5, 134–151 cm. Variables as in Figure 12.

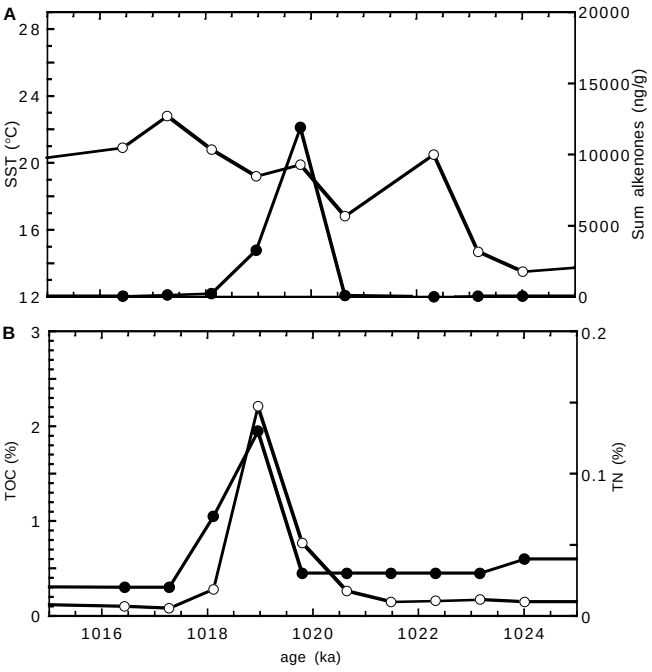

Figure 16. Plot of data for interval 160-964D-4H-5, 61–80 cm. Variables as in Figure 12.

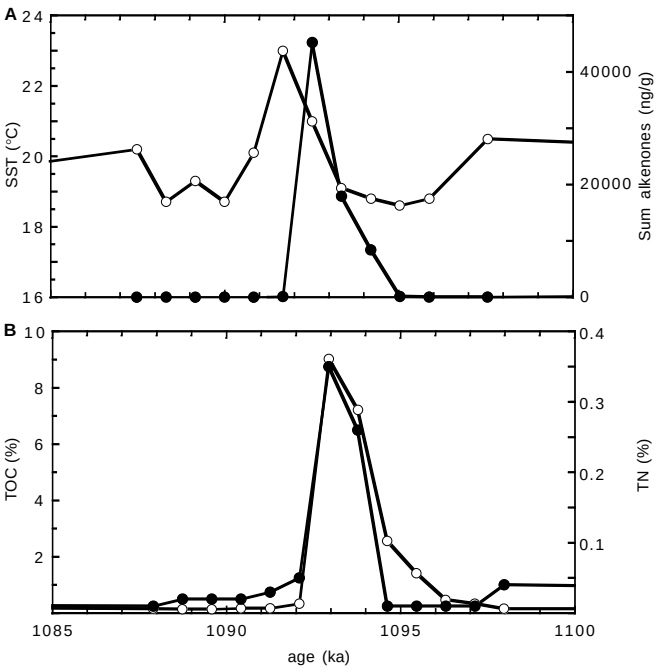

Figure 18. Plot of data for interval 160-964D-4H-6, 80–106 cm. Variables as in Figure 12.

record at Site 967 extends only to Sapropel S10. At the time of writing, sapropels from Site 964 in the Ionian Sea were being analyzed to allow us a look at salinity gradients in addition to temperature gradients.

From the lag seen between the decrease in salinity and the onset of sapropel deposition, we estimate that the reaction time of the Eastern Mediterranean Sea to an initial salinity depletion in the surface is between 600 and 1500 yr. Rohling (1994) estimates that a minimum of 360 yr are required to deplete the oxygen in the Eastern Mediterranean below 1500 m water depth at present-day productivity rates. At higher oxygen utilization rates (and productivities), the duration of the transition period from oxygenated to anoxic conditions would

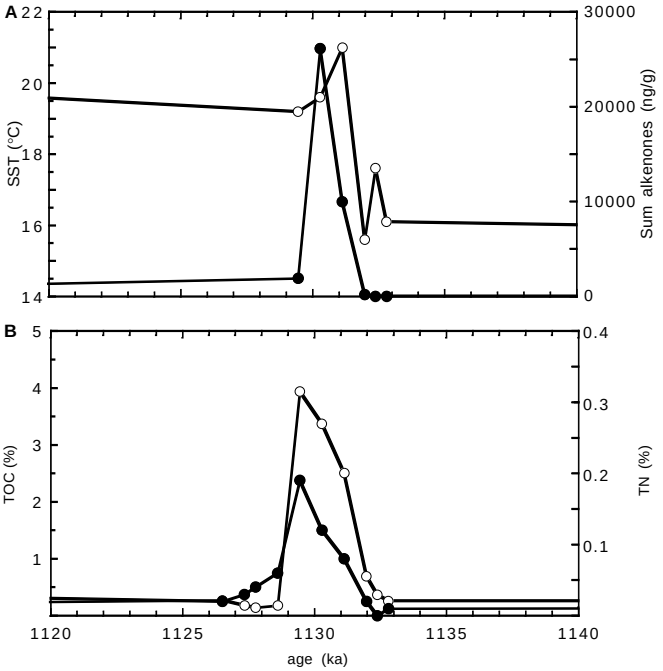

Figure 19. Plot of data for interval 160-964D-4H-7, 25–46 cm. Variables as in Figure 12.

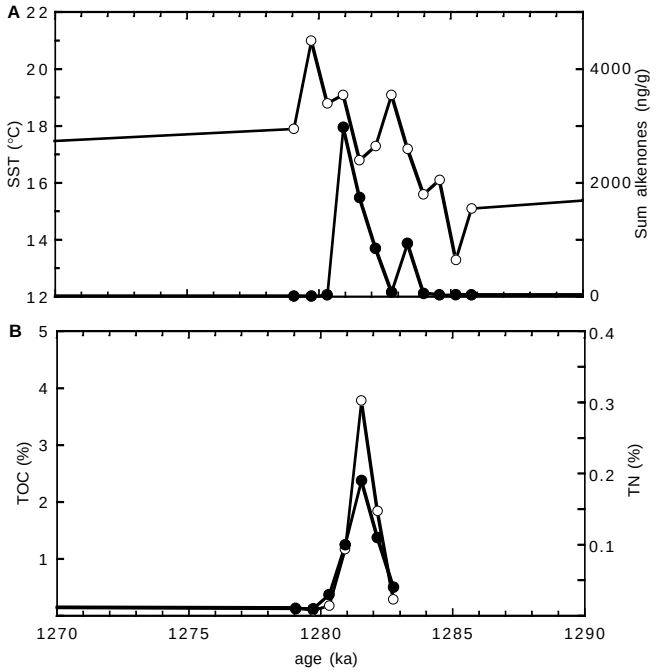

Figure 20. Plot of data for interval 160-964D-5H-2, 75–98 cm. Variables as in Figure 12.

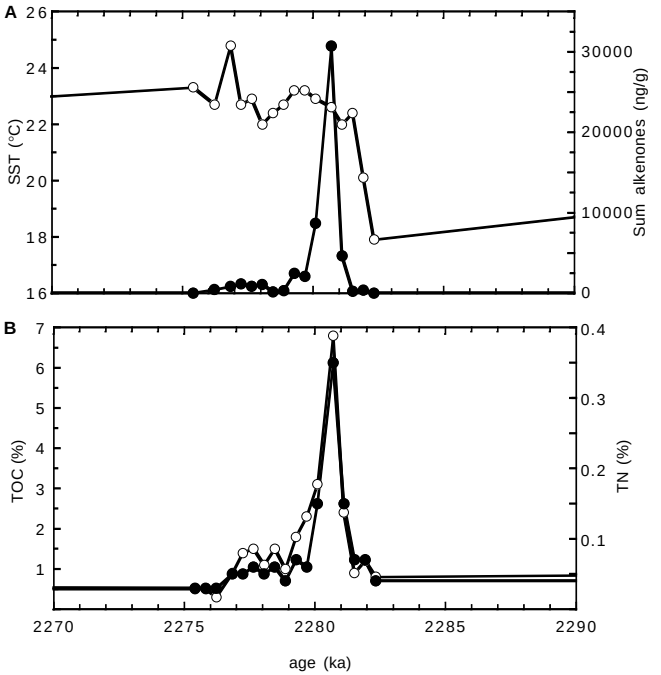

Figure 21. Plot of data for interval 160-964E-4H-2, 14–47 cm. Variables as in Figure 12.

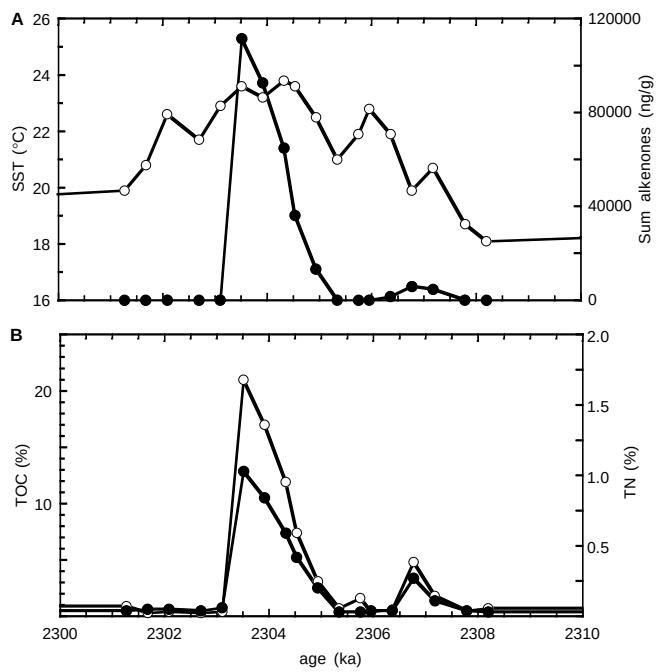

Figure 22. Plot of data for interval 160-964E-4H-2, 130 cm, to 4H-3, 15 cm. Variables as in Figure 12.

be shorter. The time difference may be explained by a gradual build-up of a low-salinity layer, which gradually spreads from the freshwater source to cover the entire basin. Explanations for the lag have been proposed by Howell and Thunell (1992) and Tang and Stott (1993), who offer different models to explain it. Our data are consistent with a freshwater source discharging into the Eastern Mediterranean Sea several thousand years before a sapropel situation is achieved. Emeis et al. (unpubl. data) evaluate a density gradient in surface seawater along an east–west series of cores for the S1 period and find that the Eastern Mediterranean surface water is less dense at an earlier time than the equivalent Ionian Basin water. They interpret this as an indication for an earlier precipitation signal in the Nile

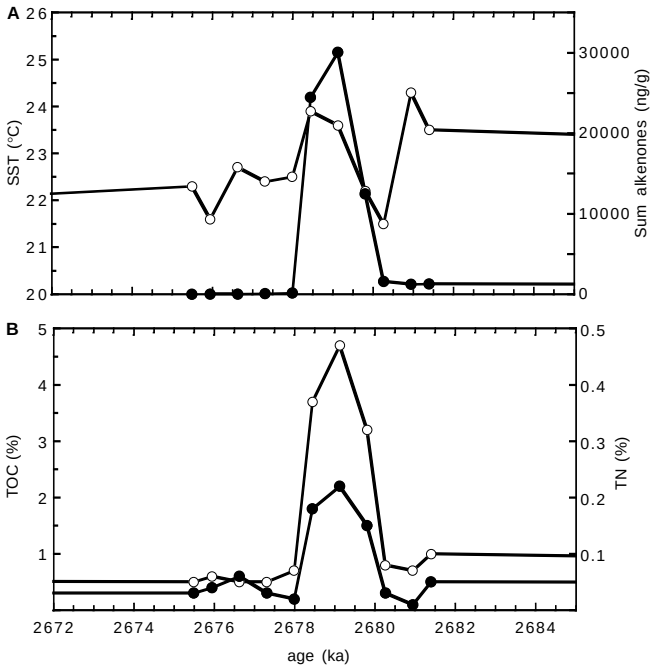

Figure 23. Plot of data for interval 160-964E-5H-5, 82–103 cm. Variables as in Figure 12.

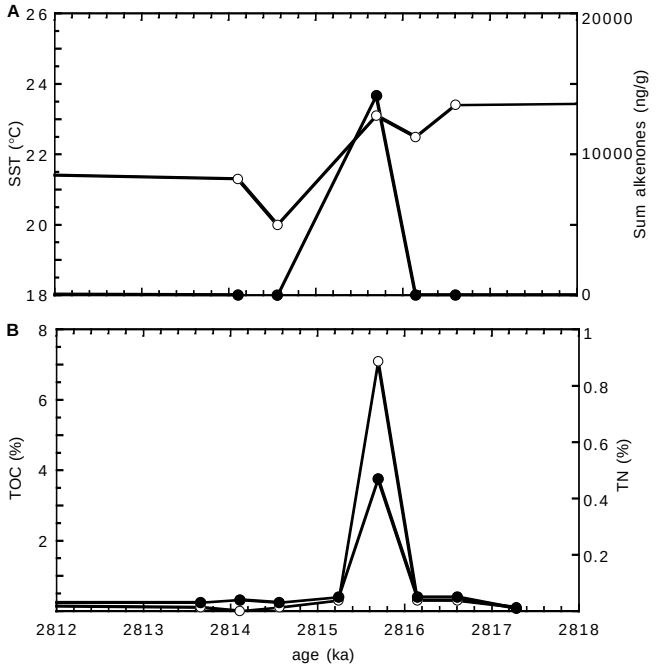

Figure 24. Plot of data for interval 160-964E-6H-2, 25–40 cm. Variables as in Figure 12.

catchment as compared to a possible northern Mediterranean borderland origin of moisture.

Comparison with Other Climate Records

Because salinity and temperatures play an important role in the stability of the water column and the generation of intermediate waters (Wüst, 1961), several attempts have been made to reconstruct paleotemperatures and paleosalinities in the Mediterranean Sea. To shed light on changes in conditions in the Mediterranean Sea on geological time scales, many researchers have used the easily accessible S1 as the test case to elucidate changes in the physical conditions (temperature and salinity) of the Mediterranean Sea. Thiede (1978) reconstructed patterns of SST based on faunal assemblages in surface sediments and sediments from the last glacial maximum (LGM). His estimate is that winter SST during LGM times ranged from 7°C to 21°C, whereas summer SST ranged from 13°C to 25°C. Distinct features of Thiede's reconstructions are tongues of cold surface waters originating from the Aegean Sea during both summer and winter under glacial conditions. In general, faunal reconstructions showed that SST in the Western and Eastern Mediterranean were on average 4°C and 6°C colder than the present SST, respectively (Thunell, 1979; Thiede, 1978). CLIMAP's (1981) reconstruction showed an increase in SST of 4°C–6°C from LGM. Based on model calculations, Bigg (1994) estimates that SST in the western basin were 3°C–4°C lower than modern during the LGM, whereas there was no significant change in the SST of most of the Eastern Mediterranean.

On longer time scales, Cita et al. (1977) interpret isotopic data of a core from the Eastern Mediterranean as an indication that temperatures have not varied by more than 8°C between glacial and interglacial stages during the late Pleistocene.

Our data suggest that even between individual periods of enhanced solar insolation and climatic optima that are represented by sapropels of the late Pleistocene group, the differences of temperatures are in excess of 8°C between cold and warm climate stages. Within sapropels, which in no case correspond to maximum glacial

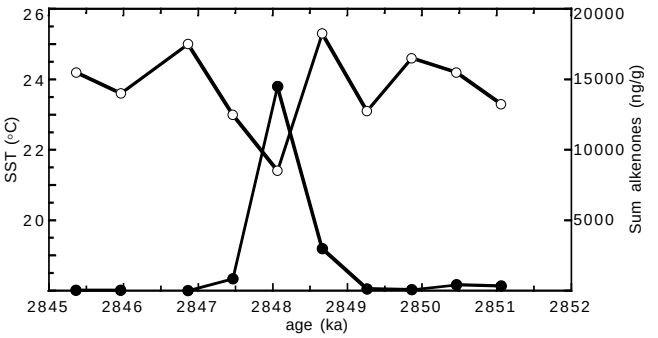

Figure 25. Plot of SST (open circles) and alkenone concentration data (solid circles) for interval 160-964E-6H-2, 125–144 cm.

conditions coupled with minimum insolation, the temperature range again is up to 8°C over periods of several hundred years. This is far more variability than expected.

The second important oceanographic variable of interest is salinity of the surface waters. Results of salinity reconstructions vary considerably. Thunell and Williams (1989) used isotope measurements on planktonic foraminifers of three time slices (LGM, 8 ka, and recent), to reconstruct salinities in the Mediterranean basins. They apply a SST correction on the average isotope ratios for each individual basin, using SST derived from faunal transfer techniques. They further subtract global ice-volume effects of 1.2‰ from the LGM values to extract residual isotope variations, which they attribute solely to salinity variations. According to their results, salinity changes in the western basin are between −1.9 and 1.2 psu, whereas salinities in the Eastern Mediterranean exceeded modern values by almost 3 psu. A similar salinity increase was found by Béthoux (1984), based on oceanographic balances. In contrast, Bigg (1994) postulates that salinities were almost unchanged. Our data for Site 967 suggest that, on

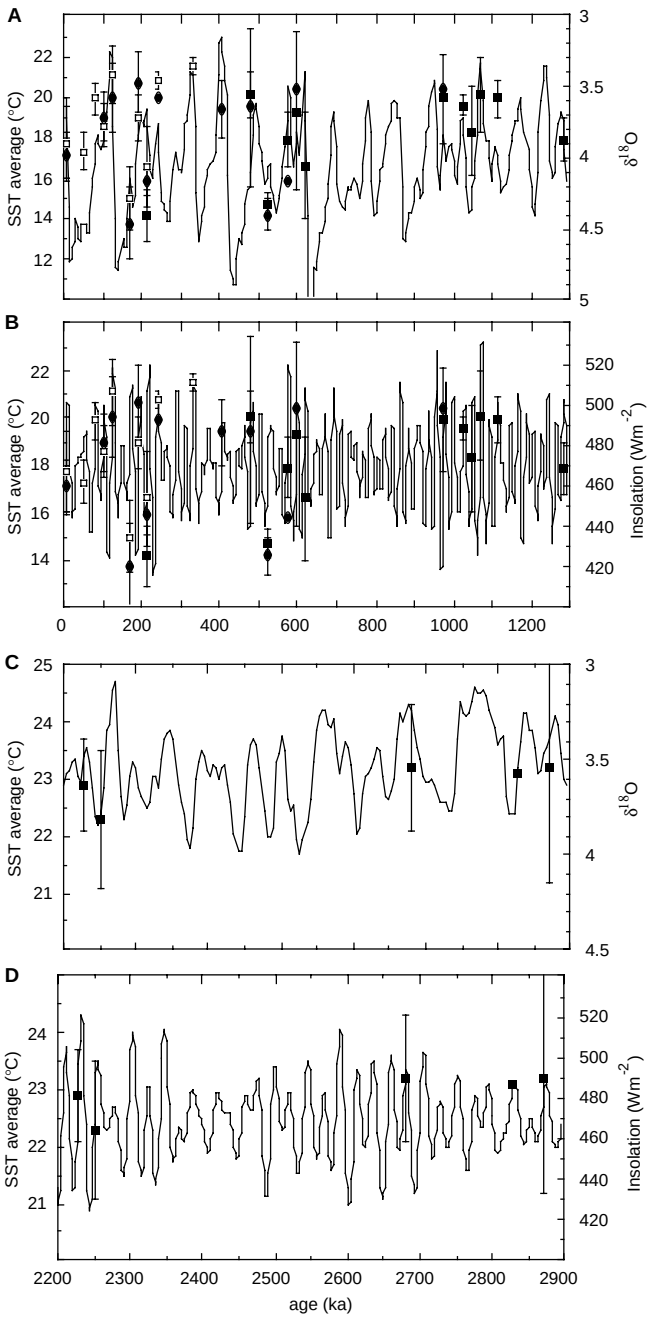

Figure 26. Average SST values of sapropels and ±1σ ranges at Site 967 (open squares), Site 964 (solid squares), and in Cores KC01/01B (solid circles) plotted against age. The data are underlain by an ice-volume record ($\delta^{18}O$ of benthic foraminifers at Site 849, equatorial East Pacific; Mix et al., 1995) in panels **A.** (0–1300 ka) and **C.** (2200–2900 ka) and by an insolation record (Laskar, 1990) in Panel **B.** (0–1300 ka) and **D.** (2200–2900 ka).

average, the salinity decrease in the sea surface mixed layer of the Levant was more than 2 psu for each of the late Pleistocene sapropels and reached up to 8 psu during some sapropel events.

In general terms, climate records from the Mediterranean are in accordance with the interpretations of the alkenone temperature records and salinity reconstructions for the sapropels investigated here. The older intervals sampled are from a time interval that is considered to predate the onset of glaciation in the northern hemisphere and the aridification of Africa (de Menocal, 1995). Dust records around Africa suggest low dust ablation before 2.8 Ma, humid climate, and precession-driven climate variability in northern Africa. The pattern of sapropel occurrence through time (e.g., Sakamoto et al., Chap. 4, this volume), as well as the temperature record at Site 964 in relation to the ice-volume and insolation records, suggest that conditions conducive to deposition of sapropels occurred regularly during almost each minimum in precession. We consider this period to be representative of an environmental setting that was consistently warmer (average of sapropels 22°C–24°C) and wetter than later environments, and one that may represent most of the Neogene.

The second interval spans the period from 1300 to 650 ka. This period contains relatively less sapropels per unit time than the older interval (Sakamoto et al., Chap. 4, this volume). It represents a situation when the global hydrological cycle had changed in response to bipolar glaciation and when desertification of Africa had proceeded. At that time the modern Mediterranean climate zonation (with a southern and southeastern catchment area influenced by subtropical aridity and the northern area influenced by polar-front depressions) may have become established. However, the high-amplitude changes evident in the benthic $\delta^{18}O$ record that signal marked increases in the glacial climate extremes have not emerged yet. Dust records from marine sequences surrounding Africa of this time interval show an imprint of high-latitude climate variability. Dust accumulation in the oceans around Africa have increased five times compared to those from 2.8 Ma and signal sustained African aridity (de Menocal, 1995). In contrast, the northern Mediterranean watershed appears to have received relatively more precipitation, and vegetation indicative of humid climates is found in terrestrial pollen records (Mommersteeg et al., 1995) during periods of sapropel deposition. The uniformly high SST averages in the sapropels from that time period show high baseline values around 20°C.

The third time period includes most of the well-known 12 sapropels that were deposited over the last 500 k.y., when the extreme fluctuations of $\delta^{18}O$ in the Mediterranean (up to 5‰) signal variability in climate and hydrography that mirrors and amplifies global climate evolution. Since that time, the terrestrial pollen records of the northern borderland are more varied and fluctuate between warm, wet climates and steppe vegetation with cool and dry climates.

CONCLUSIONS AND OUTLOOK

Our observations permit some important preliminary statements and conclusions with regard to the hypotheses listed in the Introduction.

1. SST during sapropel formation in the Eastern Mediterranean Sea varied over a range of at least 8°C in the course of the last 3 m. y. Average temperatures were very uniform at ~23°C before 2200 ka, between 18°C and 20°C from 1300 to 950 ka, and between 14°C and 22°C during the last 500 ka.
2. SST in sapropels are not related only to insolation and do not directly reflect warming from radiation during the last 500 k.y. Their baseline temperature is related to global ice volume, possibly through cooling from inland glaciers and lowered snowlines in the northern Mediterranean watershed. This situation is comparable to that found in the late Pleistocene Arabian Sea (Emeis et al., 1995).
3. A warming trend is overprinted on the background temperature level at the onset and during sapropel deposition. If the warming reflected only insolation warming, this observation would be in conflict with the finding that sapropels lag insolation maxima by 3 ka (Lourens et al., 1996). The warming trend most likely reflects a climatic amelioration with a gradual increase in baseline temperatures over a period of several centu-

Table 3. Compilation of data needed to calculate salinity changes for sapropels at Site 967.

Sapropel	Core, section, interval (cm)	Top depth (rmcd)	Age (ka)	Bottom depth (rmcd)	Age (ka)	SST_b (°C)	SST_{in} (°C)	ΔSST (°C)	T_{effect} (‰)	Ice_b (‰)	Ice_{in} (‰)	Ice_{effect} (‰)	$\delta^{18}O_b$ (‰)	$\delta^{18}O_{in}$ (‰)	$\Delta\delta^{18}O$ (‰)	$\Delta\delta^{18}O$–ΔT (‰)	$\Delta\delta^{18}O$–IE (‰)	ΔS (psu)
	160-967D-																	
S1	1-1, 110-128	1.10	8.5	1.28	10.1	13.2	18.7	5.5	-1.10	0.27	0.12	-0.15	1.21	-0.66	-1.87	-0.77	-0.62	-1.5
S2	1-3, 126-136	4.22	59.2	4.31	60.9	17.3	17.6	0.3	-0.06	0.68	0.36	-0.32	2.96	-0.47	-3.43	-3.37	-3.05	-7.4
S3	1-4, 92-97	5.38	78.9	5.42	80.7	16.5	20	3.5	-0.70	0.23	0.11	-0.12	1.28	-0.1	-1.38	-0.68	-0.56	-1.4
S4	1-4, 114-120	5.60	83.9	5.64	84.6	19.9	18.4	-1.5	0.30	0.19	0.1	-0.09	1.75	-1.19	-2.94	-3.24	-3.15	-7.7
	160-967C-																	
S5	1-5, 74-103	7.42	118.5	7.70	125.0	18.2	20	1.8	-0.36	0.05	-0.07	-0.12	-0.04	-1.91	-1.87	-1.51	-1.39	-3.4
	160-967D-																	
S6	2-1/2, 139-37	9.40	167.3	9.86	179.1	15.8	16.2	0.4	-0.08	0.53	0.65	0.12	1.4	0.73	-0.67	-0.59	-0.71	-1.7
S7	2-2/3, 134-2	10.73	201.2	10.91	207.1	19.6	19.3	-0.3	0.06	0.06	0.12	0.06	0.49	-1.94	-2.43	-2.49	-2.55	-6.2
S8	2-3, 67-103	11.55	236.5	11.78	243.0	16.9	16.8	-0.1	0.02	0.36	0.19	-0.17	-0.21	-1.25	-1.04	-1.06	-0.89	-2.2
S9	2-3/4, 147-3	12.17	251.7	12.23	253.1	16.8	20.4	3.6	-0.72	0.54	0.7	0.16	0.52	-1.02	-1.54	-0.82	-0.98	-2.4
S10	2-5, 131-138	15.02	322.1	15.07	323.6	18.6	21.1	2.5	-0.50	-0.03	-0.03	0	-0.37	-1.32	-0.95	-0.45	-0.45	-1.1

Notes: The intervals list the sapropels with elevated organic carbon/alkenone concentrations. Depths in revised meters composite depth (rmcd) are according to Sakamoto et al. (Chap. 4, this volume), ages are derived from the age model of Kroon et al. (Chap. 14, this volume). SST_b = the temperature of the sample with the highest $\delta^{18}O$ below the sapropel; SST_{in} = the samples with the lowest $\delta^{18}O$ within the sapropel. ΔSST = the temperature difference between the two samples; T_{effect} = the temperature effect on isotopic composition of this temperature difference assuming a relationship of –0.2‰ $\delta^{18}O$ per 1°C (Thunell and Williams, 1989). Ice_b = the ice volume effect at the time corresponding to the age of the sample with the highest $\delta^{18}O$ below the sapropel; Ice_{in} = the ice volume effect at the time corresponding to the sample with the lowest $\delta^{18}O$ within the sapropel. Ice volume effects have been interpolated from the data of Vogelsang (1990). Ice_{effect} = the difference in global ice volume effect from below to within the sapropel. $\delta^{18}O_b$ and $\delta^{18}O_{in}$ = the samples with the largest difference in $\delta^{18}O$ below and within the sapropel, respectively. $\Delta\delta^{18}O$ = the isotope difference between the two, $\Delta\delta^{18}O$ – ΔT = the value corrected for T_{effect}; and $\Delta\delta^{18}O$ – IE = the residual corrected for the global ice volume effect. ΔS = the residual, local salinity anomaly calculated from the remaining isotope change assuming a relationship of 0.41‰ $\delta^{18}O$ per 1 psu (Thunell and Williams, 1989).

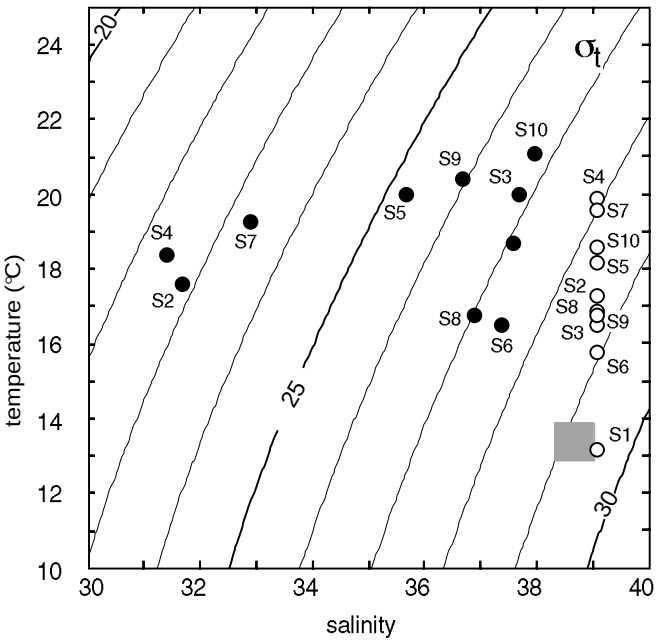

Figure 27. Temperature-salinity (T-S) diagram showing the change in the density of surface waters at Site 967 as calculated from reconstructed T and S values of late Pleistocene sapropels. The gray square is the density range occupied by intermediate water at 1500 m in the Levantine Basin today. Open circles denote values for times before sapropel deposition. Because we do not know the starting salinity (below the sapropel), we assume that it was as today (39.08). This is a minimum value due to the climatic optimum conditions in the Holocene (Béthoux, 1993). In the past, salinities are likely to have been higher before the onset of sapropel deposition, as can be deduced from the isotopic curve of $\delta^{18}O$. This would result in even denser surface waters before the inflow of lower salinity water that caused sapropel formation. Solid circles denote the T-S characteristics of individual sapropels, which were derived from SST and from subtracting ΔS (Table 3) from the starting salinity value of 39.08.

ries to millennia, possibly associated with increased precipitation. The lag of SST increase may be caused by gradual melting of inland ice in the watershed.

4. SST of different sapropels are not homogeneous, as would be expected if seasonal warming alone and physical stabilization of a stratified water column determined the onset of plankton blooms. Similarly, it is difficult to envision how SST could fluctuate as widely if massive upwelling (and concomitant decrease in SST) were the reason for sapropel formation. A temperature gradient in accordance with upwelling is not obvious in the data.
5. All sapropels investigated so far are preceded by a more or less significant decrease in salinity a few hundreds to thousands of years before the onset of organic-rich deposition. This coincides in most cases with a warming of the sea surface. The salinity at Site 967 in the Levant, an important source of intermediate water today, is between 1 and 8 psu lower during sapropel formation in the late Pleistocene. Such a salinity decrease would effectively shut down formation of intermediate waters and deep waters.

The origin of the fresher water can be located by detailed constructions of salinity gradients once the salinity of isochronous sapropels from different basins have been reconstructed. Such efforts are underway. The character of this water is also encoded in the isotope ratios of carbon and oxygen, which will require further scrutiny. Finally, it should be possible to perform volumetric calculations on the amount of water required to lower salinity in the surface mixed layer to the observed salinities. This is likely to exclude some of the sources discussed thus far for lack of mass.

ACKNOWLEDGMENTS

We acknowledge the expert alkenone analyses performed by R. Rosenberg and financial help under contract DFG Em 37/4 and EU-MAS2-CT93-0051. IOW contribution 241.

REFERENCES

Béthoux, J.P., 1984. Paléo-hydrologie de la Méditerranée au cours derniers 20000 ans. *Oceanol. Acta*, 7:43–48.

————, 1989. Oxygen consumption, new production, vertical advection and environmental evolution of the Mediterranean Sea. *Deep-Sea Res.*, 36:769–781.

————, 1993. Mediterranean sapropel formation, dynamic and climatic viewpoints. *Oceanol. Acta*, 16:127–133.

Bigg, G.R., 1994. An ocean general circulation model view of the glacial Mediterranean thermohaline circulation. *Paleoceanography*, 9:705–722.

Brassell, S.C., Eglinton, G., Marlowe, I.T., Pflaumann, U., and Sarnthein, M., 1986. Molecular stratigraphy: a new tool for climatic assessment. *Nature*, 320:129–133.

Calvert, S.E., Nielsen, B., and Fontugne, M.R., 1992. Evidence from nitrogen isotope ratios for enhanced productivity during the formation of eastern Mediterranean sapropels. *Nature*, 359:223–225.

Castradori, D., 1993. Calcareous nannofossil biostratigraphy and biochronology in eastern Mediterranean deep-sea cores. *Riv. Ital. Paleontol. Stratigr.*, 99:107–126.

Cita, M.B., Vergnaud-Grazzini, C., Robert, C., Chamley, H., Ciaranfi, N., and D'Onofrio, S., 1977. Paleoclimatic record of a long deep sea core from the eastern Mediterranean. *Quat. Res.*, 8:205–235.

CLIMAP Project Members, 1981. Seasonal reconstructions of the Earth's surface at the last glacial maximum. *Geol. Soc. Am., Map and Chart Ser.*, MC36.

Comas, M.C., Zahn, R., Klaus, A., et al., 1996. *Proc. ODP, Init. Repts.*, 161: College Station, TX (Ocean Drilling Program).

de Menocal P., 1995. Plio-Pleistocene African climate. *Science*, 270:53–59.

Emeis, K.-C., Anderson, D.M., Doose, H., Kroon, D., and Schulz-Bull, D., 1995. Sea-surface temperatures and the history of monsoon upwelling in the northwest Arabian Sea during the last 500,000 years. *Quat. Res.*, 43:355–361.

Emeis, K.-C., Doose, H., and Cacho-Lascorz, I., 1996. Reconstruction of paleotemperatures during sapropel deposition based on high-resolution analyses of geochemical biomarkers in sediments. *Unpubl. Rep. EU-MAST, MAS2-CT93-0051.*

Emeis, K.-C., and Leg 160 Shipboard Scientific Party, 1996. Paleoceanography and sapropel introduction. *In* Emeis, K.-C., Robertson, A.H.F., Richter, C., et al., *Proc. ODP, Init. Repts.*, 160: College Station, TX (Ocean Drilling Program), 21–28.

Emeis, K.-C., Robertson, A.H.F., Richter, C., et al., 1996. *Proc. ODP, Init. Repts.*, 160: College Station, TX (Ocean Drilling Program).

Hemleben, C., Spindler, M., and Anderson, O.R, 1989. *Modern Planktonic Foraminifera:* Berlin (Springer-Verlag).

Howell, M.W., and Thunell, R.C., 1992. Organic carbon accumulation in Bannock Basin: evaluating the role of productivity in the formation of Eastern Mediterranean sapropels. *Mar. Geol.*, 103:461–471.

Laskar, J., 1990. The chaotic motion of the solar system: a numerical estimate of the size of the chaotic zones. *Icarus*, 88:266–291.

Lourens, L.J., Antonarakou, A., Hilgen, F.J., Van Hoof, A.A.M., Vergnaud-Grazzini, C., and Zachariasse, W.J., 1996. Evaluation of the Plio-Pleistocene astronomical timescale. *Paleoceanography*, 11:391–413.

Miller, A.R., Tchernia, P., Charnock, H., and McGill, W.D., 1970. *Mediterranean Sea Atlas of Temperature, Salinity, Oxygen Profiles and Data from Cruises of R/V Atlantis and R/V Chain with Distribution of Nutrient Chemical Properties.* Woods Hole Oceanogr. Inst. Atlas Ser., Vol. III.

Mix, A.C., Pisias, N.G., Rugh, W., Wilson, J., Morey, A., and Hagelberg, T.K., 1995. Benthic foraminiferal stable isotope record from Site 849: 0–

5 Ma: Local and global climate changes. *In* Pisias, N.G., Mayer, L.A., Janecek, T.R., Palmer-Julson, A., and van Andel, T.H. (Eds.), *Proc. ODP, Sci. Results*, 138: College Station, TX (Ocean Drilling Program), 371–412.

Mommersteeg, H.J.P.M., Loutre, M.F., Young, R., Wijmstra, T.A., and Hooghiemstra, H., 1995. Orbial forced frequencies in the 975,000 year pollen record from Tenagi Philippon (Greece). *Clim. Dyn.*, 11:4–24.

Prahl, F.G., Muehlhausen, L.A., and Zahnle, D.L., 1988. Further evaluation of long-chain alkenones as indicators of paleoceanographic conditions. *Geochim. Cosmochim. Acta*, 52:2303–2310.

Rohling, E.J., 1994. Review and new aspects concerning the formation of eastern Mediterranean sapropels. *Mar. Geol.*, 122:1–28.

Rohling, E.J., and Gieskes, W.W.C., 1989. Late Quaternary changes in Mediterranean intermediate water density and formation rate. *Paleoceanography*, 4:531–545.

Rossignol-Strick, M., 1993. Late Quaternary climate in the Eastern Mediterranean Region. *Palaeorient.*, 19:135–152.

Rossignol-Strick, M., Nesteroff, W., Olive, P., and Vergnaud-Grazzini, C., 1982. After the deluge: Mediterranean stagnation and sapropel formation. *Nature*, 295:105–110.

Sanvoisin, R., d'Onofrio, S., Lucchi, R., Violanti, D., and Castradori, D., 1993. 1 Ma paleoclimatic record from the Eastern Mediterranean—MARFLUX project: first results of a micropaleontological and sedimentological investigation of a long piston core from the Calabrian Ridge. *Il Quaternario*, 6:169–188.

Sarmiento, J., Herbert, T., and Toggweiler, J., 1988. Mediterranean nutrient balance and episodes of anoxia. *Global Biogeochem. Cycles*, 2:427–444.

Tang, C.M., and Stott, L.D., 1993. Seasonal salinity changes during Mediterranean sapropel deposition 9000 years b.P.: evidence from isotopic analyses of individual planktonic foraminifera. *Paleoceanography*, 8:473–493.

Thiede, J., 1978. A glacial Mediterranean. *Nature*, 276:680–683.

Thunell, R. C., 1979. Eastern Mediterranean Sea during the last glacial maximum; an 18,000-years reconstruction. *Quat. Res.*, 11:353–372.

Thunell, R.C., and Williams, D.F., 1989. Glacial-Holocene salinity changes in the Mediterranean Sea: hydrographic and depositional effects. *Nature*, 338:493–496.

Thunell, R.C., Williams, D.F., and Belyea, P.R., 1984. Anoxic events in the Mediterranean Sea in relation to the evolution of late Neogene climates. *Mar. Geol.*, 59:105–134.

Vergnaud-Grazzini, C., Ryan, W.B.F., and Cita, M.B., 1977. Stable isotope fractionation, climatic change and episodic stagnation in the Eastern Mediterranean during the Late Quaternary. *Mar. Micropaleontol.*, 2:353–370.

Vogelsang, E., 1990. Paläo-Ozeanographie des Europäischen Nordmeeres an Hand stabiler Kohlenstoff-und Sauerstoffisotope [Ph.D. dissert.]. Christian-Albrechts-Univ. zu Kiel.

Williams, D.F., and Thunell, R.C., 1979. Faunal and oxygen isotopic evidence for surface water salinity changes during sapropel formation in the eastern Mediterranean. *Sediment. Geol.*, 23:81–93.

Wüst, G., 1961. Das Bodenwasser und die Vertikalzirkulation des Mittelländischen Meeres. *Dtsch. Hydrogr. Z.*, 14:81–92.

Date of initial receipt: 15 January 1997
Date of acceptance: 19 June 1997
Ms 160SR-011